Convergence of H(div)-conforming schemes for a new model of sedimentation in circular clarifiers with a rotating rake

Raimund Bürger[a], Paul E. Méndez[a], Ricardo Ruiz-Baier[b,c,*]

[a] *CI²MA and Departamento de Ingeniería Matemática, Universidad de Concepción, Casilla 160-C, Concepción, Chile*
[b] *School of Mathematics, Monash University, 9 Rainforest Walk, Clayton, Victoria 3800, Australia*
[c] *Laboratory of Mathematical Modelling, Institute of Personalised Medicine, Sechenov University, Moscow, Russian Federation*

Abstract

A macroscopic model is introduced for simulating the sedimentation–consolidation of solid particles in an incompressible fluid under the effect of gravity and in the presence of a slowly rotating arm assisting the removal of sediment on the bottom of clarifier–thickener units. The governing model is an initial–boundary value problem for the Navier–Stokes equations describing the flow of the mixture coupled with a nonlinear parabolic equation describing the volume fraction of solids. The rotating structure is accounted for by suitable drag laws on the momentum balance of the mixture and on the mass balance of the solid phase. An H(div)-conforming method for the coupled problem is proposed, a rigorous proof of convergence is provided, and the validity of the new model and the performance of the scheme are demonstrated numerically by several computational tests.
© 2020 Elsevier B.V. All rights reserved.

1. Introduction

1.1. Scope

We advance a phenomenological model of solid–fluid interaction in a continuously operated clarifier–thickener, which is an equipment widely used in the mining industry, wastewater treatment plants, and other applications. The new continuum–based model accounts for the effect of the rotating rake structure, the influence of the settling solid particles, and the three-dimensional incompressible flow of the mixture. A large variety of these devices are used in industry, but most clarifier–thickeners are circular tanks of 1.5 m to 150 m in diameter equipped with a feed inlet and overflow and discharge outlets for continuous operation. In many devices, a pair of rotating rake arms that move over the gently sloped bottom help to move the concentrated slurry towards the centre of the tank, where

---

* Correspondence to: School of Mathematics, Monash University, 9 Rainforest Walk, Clayton, Victoria 3800, Australia.
 E-mail addresses: rburger@ing-mat.udec.cl (R. Bürger), pmendez@ci2ma.udec.cl (P.E. Méndez), ricardo.ruizbaier@monash.edu (R. Ruiz-Baier).
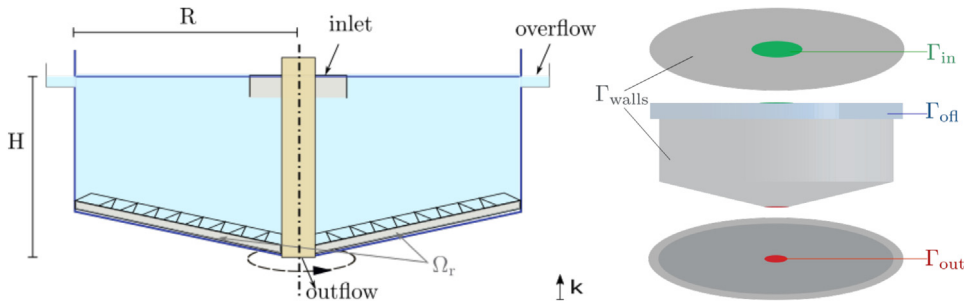
Fig. 1.1. Left: schematic view of the clarifier unit, indicating height H, maximal radius R, and the location of the rotating rake. Right: separation of the boundary into the walls, the outlet, the feedwell inlet, and the overflow weir.

it is removed. Clear liquid overflows the top of the tank and is collected through a circumferential launder (see Fig. 1.1). Although there are many main types of thickeners or clarifiers such as bridge support, column support, and traction devices, for the purpose of the present modelling framework these are all considered equivalent.

The mathematical modelling and numerical simulation of this kind of processes is challenging due to the intrinsic multiscale and highly nonlinear nature of the sedimentation–consolidation mechanisms, complicated geometries and boundary conditions, as well as the feedback interaction between the mixture flow and the motion of the rake (the fluid applies a load on the solid structure, implying a deformation, generating stresses, and eventually modifying the flow). For instance, simplified models that would be based on geometrical symmetry are in this case of very restricted applicability, since the settling of the particles occurs in the vertical direction while the rotation of the rake acts in two horizontal directions, and the velocity distribution under typical operating conditions is quite far from unidirectional.

We consider the process of sedimentation and transport of a suspension consisting of a phase of finely divided solid particles dispersed in a viscous fluid. This mixture is contained in a clarifier tank with a moving rake. For the sedimentation–consolidation of the suspension we assume that the particles are relatively small with respect to the tank size and possess the same density. It is assumed that the mixture is composed of incompressible solid and liquid phases, that the mixture velocity is relatively small, and that the suspension is already flocculated before the process starts (see [1,2]). The motion of the mixture is governed by the incompressible Navier–Stokes equations coupled with the transport equation for the solids as follows:

$$\rho_{\mathrm{f}}\left(\frac{\partial \boldsymbol{u}}{\partial t} + \mathbf{div}(\boldsymbol{u} \otimes \boldsymbol{u})\right) - \mathbf{div}\big(\nu(c)\boldsymbol{\varepsilon}(\boldsymbol{u})\big) + \nabla p = \boldsymbol{f}_{\mathrm{g}}(c) + \boldsymbol{f}_{\mathrm{r}}(\boldsymbol{u}, \boldsymbol{x}, t), \tag{1.1a}$$

$$\mathrm{div}\,\boldsymbol{u} = 0, \tag{1.1b}$$

$$\frac{\partial c}{\partial t} - \mathrm{div}\big(D(c)\nabla c - c\boldsymbol{u} - f_{\mathrm{bk}}(c)\boldsymbol{k}\big) = -g_{\mathrm{r}}(c, \boldsymbol{x}, t) \quad \text{in } \Omega \times (0, T]. \tag{1.1c}$$

Here the sought quantities are the mixture velocity $\boldsymbol{u}$, the pressure p and the local solids fraction c as functions of time $t \in [0, T]$ and spatial position $\boldsymbol{x} \in \Omega \subset \mathbb{R}^3$, where the spatial domain Ω represents the interior of the clarifier–thickener. Moreover, ρ_{f} is the fluid density, $\boldsymbol{\varepsilon}(\boldsymbol{u}) = \frac{1}{2}(\nabla \boldsymbol{u} + \nabla \boldsymbol{u}^{\mathrm{T}})$ is the strain rate tensor, and $\boldsymbol{k}$ is the upwards-pointing unit vector. The material behaviour is described by the concentration-dependent viscosity ν, the Kynch batch flux density function f_{bk}, and the diffusion function D. These three quantities are nonlinear given functions of c that are specified in Section 2.1. The term $\boldsymbol{f}_{\mathrm{g}}(c)$ represents the body force and is given by $\boldsymbol{f}_{\mathrm{g}}(c) = \boldsymbol{g}\,(\rho_{\mathrm{s}} - \rho_{\mathrm{f}})\,c$ as in [3], where $\boldsymbol{g} = -g\boldsymbol{k}$ and g is the acceleration of gravity. The terms $\boldsymbol{f}_{\mathrm{r}}(\boldsymbol{u}, \boldsymbol{x}, t)$ and $g_{\mathrm{r}}(c, \boldsymbol{x}, t)$ describe the action of the rotating rake, and are specified in Section 2.2. The system (1.1) is supplied with initial and boundary conditions that are made precise in Section 2.3.

It is the purpose of this paper to advance a novel discretisation for the resulting initial–boundary value problem that is of second-order in space and time. The discretisation employs divergence-conforming Brezzi–Douglas–Marini (BDM) elements of order k for the approximation of the velocity, discontinuous elements of order $k - 1$ for the pressure, and continuous Lagrange elements of order k for the volume fraction. We use an interior penalty discontinuous Galerkin technique in order to enforce $\mathbf{H}^1$-continuity of the velocity (similarly to what is done in [4]);

and employ the second-order backward differentiation formula (BDF2) for the discretisation in time. Our analysis includes the stability of solutions of the associated Galerkin scheme and the derivation of optimal error estimates in time and space for problems with small and sufficiently smooth solutions. These properties constitute a proof of convergence of the fully discrete scheme as the mesh width and the time step tend to zero. The novelty of the treatment consists in the inclusion of terms that account for the influence of the rake motion on the momentum balance and the removal of solids. We also adapt techniques of the immerse boundary finite element method (see e.g. [5]) for the analysis and numerical approximation of those terms.

1.2. Related work

Early models for the clarifying process with and without swirl effects were reviewed in [6], where mainly axisymmetric configurations were employed. More recently, a fairly complete model can be found in [3], where the authors couple the momentum equations for fluid flow with a transport equation for solids. The realisable $k - \epsilon$ model, in conjunction with scalable wall functions, is used to model turbulence. The removal of sludge from the clarifier floor by means of a spinning rake is modelled through a rotating sink term added to the right-hand side of the transport equation. References that are related to the rake mechanism in applications of mineral processing include [7–14]; see Section 5 for further discussion.

Here we also include appropriate drag terms, much as in [15], that account for the indirect effects of the rake on the flow patterns. This consists basically in penalising the moving structure and computing (or as we do here, simply imposing) its velocity and its reconfiguration in an adequate manner. Volume penalisation techniques can be frequently found in the relevant literature. See, for instance, [16,17], where the authors propose high-order methods for the modelling of solid obstacles as porous structures whose permeability tends to zero and the flow is regarded in a unified domain, and the momentum on the obstacle is simply obtained from integration of the penalised velocity over the obstacle domain. Other modelling and numerical approaches one could use to incorporate the interaction between the rake and the flow include immerse boundary and fictitious domain finite elements [18], level set methods and their variants [19,20], other unfitted finite element schemes [21]; or formulations based on remodelling, such as the arbitrary Lagrangian–Eulerian (ALE) setting [22]. In summary, the main advantage in the present model with respect to the motivating problem from [3] is the inclusion of a two-way flow-transport coupling and the rake mechanism on the momentum balance equation. In contrast, our model does not include a dedicated sub-model for capturing small Kolmogorov scales and turbulent regimes.

Moreover, we emphasise that the fluid–structure interaction considered in [22] is more involved than the present approach since the elastic deformation of the rotating structure by the moving fluid is explicitly modelled. The fluid itself is considered Newtonian and incompressible described by the Navier–Stokes equations while in the present approach, and in the application, the evolution of the solids volume fraction (modelled by the transport equation) is important. This volume fraction also affects the (effective) viscosity of the fluid. On the other hand, Rudman et al. [12] focus on the technological aspect of rotating rakes, including experimental results and simulations by computational fluid dynamics (CFD). They analysed the yield stress of the suspension in relation to the rake torque, with a focus on the effect of size and shape of the rake blades. Their simulations were made for a single-phase fluid with Herschel–Bulkley rheology. Contrary to the present approach, no dewatering was considered in [12].

1.3. Outline of the paper

We have organised the contents of this paper in the following manner. Section 2 describes the general governing equations, the constitutive relations, and the interaction terms. It also specifies the boundary and initial conditions, and it outlines the weak formulation of the problem for a fixed time. In Section 3 we introduce the Galerkin discretisation and define the fully discrete method, briefly addressing stability and convergence properties. Section 4 is devoted to the computational results, including parameter calibration, accuracy verification, as well as the simulation of clarifier performance under different operation scenarios. We close the paper with some remarks and discussions given in Section 5.
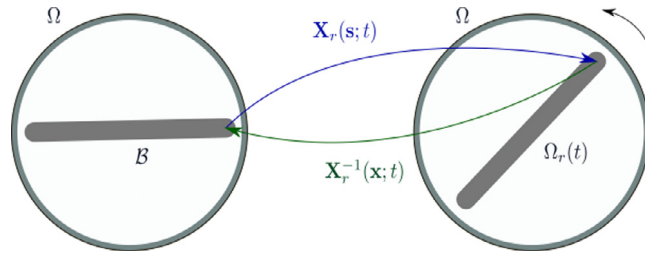
Fig. 2.1. Schematic representation of the mapping $\mathbf{X}_r$ from the rake reference domain $\mathcal{B}$ to the moving domain $\Omega_r(t)$ in a longitudinal section of the clarifier unit.

2. Preliminaries

2.1. Constitutive functions

The viscosity ν is supposed to be given by the following nonlinear function of c:

$$\nu(c) = \nu_0 + \nu_0(1 - c/c_{\max})^b, \tag{2.2}$$

where ν_0 is the viscosity of the pure fluid, $b > 0$ is a parameter, and $c_{\max}$ is a (nominal) maximum solids volume fraction. We do not consider here the high-order terms that account for microstructural arrangement of the granular material as e.g. in [2]. Moreover, the one-dimensional Kynch batch flux density function f_{bk} describing hindered settling [23] and the sediment compressibility $D(c)$ are nonlinear functions of the concentration c that can be chosen as follows [24]:

$$f_{\mathrm{bk}}(c) = u_\infty \left[c \left(1 - \frac{c}{c_{\max}} \right)^{\eta_F} \right], \quad D(c) = D_0 + \frac{f_{\mathrm{bk}}(c)\sigma_{\mathrm{e}}'(c)}{(\rho_{\mathrm{s}} - \rho_{\mathrm{f}})gc}, \tag{2.3}$$

where u_∞ is the Stokes velocity, η_F a material-dependent exponent, $D_0 > 0$ is the constant of hydrodynamic self-diffusion, ρ_{s} and ρ_{f} are the solid and fluid mass densities, respectively, and $\sigma_{\mathrm{e}}(c)$ is the so-called effective solid stress function, which characterises sediment compressibility in the case of flocculated particles. The function σ_{e} is assumed to satisfy $\sigma_{\mathrm{e}}'(c) = \mathrm{d}\sigma_{\mathrm{e}}(c)/\mathrm{d}c \geq 0$ for all c, which ensures that $D(c) \geq D_0 > 0$.

2.2. Rotating rake

To include the rotating rake into the computational model, we follow Das et al. [3] using a simplified approach that only takes into account the area of influence of the rake, and characterises the details of its geometry through parameters. The rake area of influence (hereinafter we will refer to it only as rake) $\Omega_r(t)$ can be represented as the image of a mapping $\mathbf{X}_r(\cdot; t)$ from a reference domain $\mathcal{B} \subset \mathbb{R}^d$ (see Fig. 2.1). We denote by s the coordinates in $\mathcal{B}$, then $\mathbf{X}_r(s; t)$ represents the position of a point in the current domain $\Omega_r(t)$. That is, $x \in \Omega_r(t)$ if and only if there exists $s \in \mathcal{B}$ such that $x = \mathbf{X}_r(s; t)$. For simplicity we will consider a constant angular velocity ω for the rake, then the rake velocity $\boldsymbol{u}_{\mathrm{r}}(s)$ depends only on the distance to the rake centre. Further, we suppose $\boldsymbol{f}_{\mathrm{r}}$ depends on the difference between the fluid velocity and the rake velocity $\boldsymbol{u}_{\mathrm{r}}$ and g_{r} depends on the difference between the concentration in front of the rake and a concentration after removal c_{r}, which is linked to the rake geometry. To express $\boldsymbol{f}_{\mathrm{r}}(\boldsymbol{u}, \boldsymbol{x}, t)$ in compact form, it is useful to define the function $\zeta : \mathbb{R} \to \mathbb{R}$ given by $\zeta(x) = x^2 \operatorname{sgn} x = x|x|$. Then we define

$$\boldsymbol{f}_{\mathrm{r}}(\boldsymbol{u}, \boldsymbol{x}, t) := \begin{cases} \beta \rho_{\mathrm{r}} \zeta \big((\boldsymbol{u}_{\mathrm{r}}(\mathbf{X}_r^{-1}(\boldsymbol{x}; t)) - \boldsymbol{u}(\boldsymbol{x}, t)) \cdot \boldsymbol{n}_{\mathrm{r}} \big) \boldsymbol{n}_{\mathrm{r}} & \text{if } \boldsymbol{x} \in \Omega_r(t), \\ \boldsymbol{0} & \text{otherwise,} \end{cases} \tag{2.4}$$

$$g_{\mathrm{r}}(c, \boldsymbol{x}, t) := \begin{cases} \alpha \big(c(\boldsymbol{x}, t) - c_{\mathrm{r}} \big) & \text{if } \boldsymbol{x} \in \Omega_r(t), \\ 0 & \text{otherwise,} \end{cases} \tag{2.5}$$

where α is a removal coefficient, β is the drag coefficient that includes the contact surface to volume ratio, ρ_{r} the rake density and $\boldsymbol{n}_{\mathrm{r}}$ the vector pointing towards the tangential direction with respect to the circular motion of the

rake in the (x_1, x_2)-plane. With respect to the chosen algebraic forms of the functions $\boldsymbol{f}_r$ and $\boldsymbol{g}_r$ we mention that in principle any functions representing rake rotation could be employed as long as they are supported on the rake, that is, the moving domain $\Omega_r(t)$, as in the case of the choices (2.4) and (2.5). This property ensures that these expressions can be rewritten in a particular form (involving the Dirac delta function) that follows the approach of the immersed boundary method [5,18]. However, for our convergence analysis, we will also require the variational forms derived from these terms to satisfy properties (3.24) and (3.27), which in practice restricts the form that these expressions can adopt. The physical considerations leading to the particular algebraic form (2.4) are outlined above, and are inspired by a recent model of solid–fluid interaction within a model of flow through a submerged canopy [15]. In fact, (2.4) is a term describing the momentum loss due to drag that has been adopted from [15, Eq. (2.4a)]. On the other hand, our choice of g_r is motivated by the same expression arising as a rotating sink term in [3] (cf. Eq. (13)) of that paper. With the consistency with the analyses of [5,18] in mind, we now rewrite (2.4) and (2.5) as follows:

$$\boldsymbol{f}_r(\boldsymbol{u}, \boldsymbol{x}, t) = \beta \rho_r \int_{\mathcal{B}} \zeta\big(\boldsymbol{u}_r(s) - \boldsymbol{u}(\mathbf{X}_r(s, t); t) \cdot \boldsymbol{n}_r\big) \boldsymbol{n}_r \delta\big(\boldsymbol{x} - \mathbf{X}_r(s; t)\big)\, ds,$$

$$g_r(c, \boldsymbol{x}, t) = \alpha \int_{\mathcal{B}} \big(c(\mathbf{X}_r(s, t); t) - c_r\big) \delta\big(\boldsymbol{x} - \mathbf{X}_r(s; t)\big)\, ds \quad \text{for all } \boldsymbol{x} \in \Omega \text{ and } t \in (0, T].$$

(2.6)

Here, δ is the Dirac delta function, and we stress that even if the presence of the rotating arm through (2.6) does not resolve stress localisation on the structure, it already represents an extension over the model in [3].

2.3. Initial and boundary conditions

The set of governing equations is furnished with the following initial and boundary conditions:

$$\boldsymbol{u}(0) = \boldsymbol{0}, \quad c(0) = c_0 \qquad \text{in } \Omega, \tag{2.7a}$$

$$\boldsymbol{u}(\boldsymbol{x}, t) = \boldsymbol{u}_{\text{in}} \qquad \text{on } \Gamma_{\text{in}}, \, t \in [0, T], \tag{2.7b}$$

$$c(\boldsymbol{x}, t) = c_{\text{in}} \qquad \text{on } \Gamma_{\text{in}}, \, t \in [0, T], \tag{2.7c}$$

$$\boldsymbol{u}(\boldsymbol{x}, t) = \boldsymbol{0} \qquad \text{on } \Gamma_{\text{wall}}, \, t \in [0, T], \tag{2.7d}$$

$$[\nu(c)\boldsymbol{\varepsilon}(\boldsymbol{u}) - p\mathbf{I}]\boldsymbol{n} = \boldsymbol{0} \qquad \text{on } \Gamma_{\text{out}} \cup \Gamma_{\text{ofl}}, \, t \in [0, T], \tag{2.7e}$$

$$(D(c)\nabla c - f_{\text{bk}}(c)\boldsymbol{k}) \cdot \boldsymbol{n} = 0 \qquad \text{on } \Gamma_{\text{wall}} \cup \Gamma_{\text{in}}, \, t \in [0, T], \tag{2.7f}$$

$$D(c)\nabla c \cdot \boldsymbol{n} = 0 \qquad \text{on } \Gamma_{\text{out}} \cup \Gamma_{\text{ofl}}, \, t \in [0, T], \tag{2.7g}$$

which represent that at the inlet we impose velocity and volume fraction of solids, on the walls we set no-slip velocity and zero-flux for c, and on the outlet and effluent overflow regions we set zero normal total stress, and zero total flux. The disposition of domain boundaries is exemplified in Fig. 1.1.

2.4. Weak formulation

We shall use standard notation for function spaces. So, for instance, $L^p(\Omega)$, $W^{m,p}(\Omega)$, will denote the usual Lebesgue and Sobolev spaces on the domain Ω, with norms $\|\cdot\|_{p,\Omega}$ and $\|\cdot\|_{m,p,\Omega}$, respectively. We denote by $L^s(0, T; W^{m,p}(\Omega))$ the parabolic Bochner space of all L^s-integrable functions from $[0, T]$ into $W^{m,p}(\Omega)$ with norm

$$\|v\|_{L^s(0,T;W^{m,p}(\Omega))} = \left(\int_0^T \|v\|_{W^{m,p}(\Omega)}^s \, dt \right)^{1/s}.$$

By $\mathbf{L}$ and $\mathbb{L}$ we denote the corresponding vectorial and tensorial counterparts of the scalar functional space L.

The weak formulation of problem (1.1) is obtained by testing against suitable functions and integrating by parts, and can be stated as follows:

Find $(\boldsymbol{u}(t), p(t), c(t)) \in \mathbf{H}^1(\Omega) \times L^2(\Omega) \times H^1(\Omega)$ satisfying

the boundary conditions (2.7b) and (2.7c) and for all $\boldsymbol{v} \in \mathbf{H}_0^1(\Omega)$, $q \in L^2(\Omega)$ and $l \in H^1(\Omega)$:

$$\big(\partial_t \boldsymbol{u}(t), \boldsymbol{v}\big)_\Omega + a_1\big(c(t); \boldsymbol{u}(t), \boldsymbol{v}\big) + c_1\big(\boldsymbol{u}(t); \boldsymbol{u}(t), \boldsymbol{v}\big) - b\big(\boldsymbol{v}, p(t)\big) = \mathbf{F}_g(c(t), \boldsymbol{v}) + \mathbf{F}_r(\boldsymbol{u}(t), \boldsymbol{v}),$$

$$b\big(\boldsymbol{u}(t), q\big) = 0,$$

$$\big(\partial_t c(t), l\big)_\Omega + a_2\big(c(t); c(t), l\big) + c_2\big(\boldsymbol{u}(t); c(t), l\big) - d_2\big(c(t), l\big) = -G_r\big(c(t), l\big).$$

(2.8)

Using [5, Lemma 1], we can consider $\mathbf{F}_r \in \mathbf{H}^{-1}(\Omega)$, $G_r \in H^{-1}(\Omega)$, and the variational forms that are defined as follows for all $\boldsymbol{u}, \boldsymbol{v}, \boldsymbol{w} \in \mathbf{H}^1(\Omega)$, $q \in L^2(\Omega)$, and $c, l \in H^1(\Omega)$:

$$a_1(c; \boldsymbol{u}, \boldsymbol{v}) := \big(\nu(c)\boldsymbol{\varepsilon}(\boldsymbol{u}), \, \boldsymbol{\varepsilon}(\boldsymbol{v})\big)_\Omega, \quad b(\boldsymbol{v}, q) := (q, \operatorname{div}\boldsymbol{v})_\Omega, \quad c_1(\boldsymbol{w}; \boldsymbol{u}, \boldsymbol{v}) := \big((\boldsymbol{w} \cdot \nabla)\boldsymbol{u}, \, \boldsymbol{v}\big)_\Omega,$$

$$\mathbf{F}_g(c, v) = \big(\boldsymbol{g}\,(\rho_f - \rho_s)\,c, \, \boldsymbol{v}\big)_\Omega,$$

$$\mathbf{F}_r(\boldsymbol{u}, \boldsymbol{v}) = \beta\rho_r \int_{\mathcal{B}} \zeta\big((\boldsymbol{u}_r(\boldsymbol{s}) - \boldsymbol{u}(\mathbf{X}_r(\boldsymbol{s}; t), t)) \cdot \boldsymbol{n}_r\big) \boldsymbol{n}_r v\big(\mathbf{X}_r(\boldsymbol{s}; t)\big) \, \mathrm{d}s,$$

$$a_2(c; c, l) := \big(D(c)\nabla c, \, \nabla l\big)_\Omega, \quad c_2(\boldsymbol{v}; c, l) := (\boldsymbol{v} \cdot \nabla c, \, l)_\Omega,$$

$$d_2(c, l) = \big(f_{\mathrm{bk}}(c)\boldsymbol{k}, \, \nabla l\big)_\Omega - \langle f_{\mathrm{bk}}(c)\boldsymbol{k} \cdot \boldsymbol{n}, \, l\rangle_{\Gamma_{\mathrm{out}} \cup \Gamma_{\mathrm{ofl}}}, \quad G_r(c, l) := \alpha \int_{\mathcal{B}} \big(c(\mathbf{X}_r(\boldsymbol{s}; t), t) - c_r\big) l\big(\mathbf{X}_r(\boldsymbol{s}; t)\big) \, \mathrm{d}s.$$

Although some related results are available from the literature, for instance the existence of strong and weak solutions for the periodic motion of a rigid body in an incompressible fluid [25], the solvability analysis of (2.8) for the 3D case is still an open problem. We will proceed to the semidiscrete analysis under the assumption that the continuous problem possesses a sufficiently regular weak solution, also supposing that such solution is unique within a certain radius. In particular, these assumptions permit the derivation of error estimates for the discrete approximations defined in what follows.

3. Numerical method

3.1. Definition of the discrete problem

For the space discretisation we consider a family of regular partitions, denoted $\mathcal{T}_h$, of $\Omega \subset \mathbb{R}^d$ into elements K (triangles in 2D or tetrahedra in 3D) of diameter h_K. The mesh size (the maximum of these diameters) is denoted by h, and for any interior facet e in $\mathcal{E}_h$ (the set of faces in $\mathcal{T}_h$), we label K^- and K^+ the elements adjacent to it, while h_e stands for the length of edge e in 2D (or maximum diameter of the facet in 3D). Suppose that $\boldsymbol{v}$ and w are smooth vector and scalar fields, respectively, defined on $\mathcal{T}_h$. Then we denote by $(\boldsymbol{v}^\pm, w^\pm)$ the traces of $(\boldsymbol{v}, w)$ on e that are the extensions from the interiors of the elements K^+ and K^-, respectively. Let $\boldsymbol{n}_e^\pm$ denote the outward unit normal vector to e on $K^\pm$ (hence, $\boldsymbol{n}^+ = -\boldsymbol{n}^-$). We define the average $\{\!\{\cdot\}\!\}$ and jump $[\![\cdot]\!]$ operators as $\{\!\{\boldsymbol{v}\}\!\} := (\boldsymbol{v}^- + \boldsymbol{v}^+)/2$, $\{\!\{w\}\!\} := (w^- + w^+)/2$, $[\![\boldsymbol{v}]\!] := (\boldsymbol{v}^- - \boldsymbol{v}^+)$ and $[\![w]\!] := (w^- - w^+)$, whereas for boundary jumps and averages we adopt the convention that $\{\!\{\boldsymbol{v}\}\!\} = [\![\boldsymbol{v}]\!] = \boldsymbol{v}$ and $\{\!\{w\}\!\} = [\![w]\!] = w$. In addition, we denote by ∇_h the broken gradient operator.

For $k \geq 1$ and a mesh $\mathcal{T}_h$ on Ω, let us consider the discrete spaces (see e.g. [4,26])

$$\mathbf{V}_h := \big\{\boldsymbol{v}_h \in \mathbf{H}(\operatorname{div}; \Omega) : \boldsymbol{v}_h|_K \in [\mathbb{P}_k(K)]^d \quad \forall K \in \mathcal{T}_h\big\},$$

$$\mathcal{Q}_h := \big\{q_h \in L^2(\Omega) : q_h|_K \in \mathbb{P}_{k-1}(K) \quad \forall K \in \mathcal{T}_h\big\},$$

$$\mathcal{M}_h := \big\{s_h \in C(\bar{\Omega}) : l_h|_K \in \mathbb{P}_k(K) \quad \forall K \in \mathcal{T}_h\big\},$$

which in particular satisfy $\operatorname{div}\mathbf{V}_h \subset \mathcal{Q}_h$ (cf. [27]). Here $\mathbb{P}_k(K)$ denotes the local space spanned by polynomials of degree up to k and $\mathbf{V}_h$ is the space of divergence-conforming BDM elements. Associated with these finite-dimensional spaces, we state the following semi-discrete Galerkin formulation for problem (1.1):

Find $(\boldsymbol{u}_h, p_h, c_h) \in \mathbf{V}_h \times \mathcal{Q}_h \times \mathcal{M}_h$ such that for all $(\boldsymbol{v}_h, q_h, l_h) \in \mathbf{V}_h \times \mathcal{Q}_h \times \mathcal{M}_h$:

$$\begin{aligned}
&(\partial_t \boldsymbol{u}_h, \boldsymbol{v}_h)_\Omega + a_1^h(c_h; \boldsymbol{u}_h, \boldsymbol{v}_h) + c_1^h(\boldsymbol{u}_h; \boldsymbol{u}_h, \boldsymbol{v}_h) - b(\boldsymbol{v}_h, p_h) = \mathbf{F}_g(c_h, v_h) + \mathbf{F}_r(\boldsymbol{u}_h, \boldsymbol{v}_h), \\
&b(\boldsymbol{u}_h, q_h) = 0, \\
&(\partial_t c_h, l_h)_\Omega + a_2(c_h; c_h, l_h) + c_2(\boldsymbol{u}_h; c_h, l_h) - d_2(c_h, l_h) = -G_r(c_h, l_h).
\end{aligned} \tag{3.9}$$

Here the discrete versions of the trilinear forms $a_1^h(\cdot; \cdot, \cdot)$ and $c_1^h(\cdot; \cdot, \cdot)$ are defined using a symmetric interior penalty and an upwind approach, respectively (see e.g. [27,28]):

$$\begin{aligned}
a_1^h(c_h; \boldsymbol{u}_h, \boldsymbol{v}_h) := &\int_\Omega \big(\nu(c_h)\boldsymbol{\varepsilon}_h(\boldsymbol{u}_h) : \boldsymbol{\varepsilon}_h(\boldsymbol{v}_h)\big) \\
&+ \sum_{e \in \mathcal{E}_h} \int_e \Big(-\{\!\{\nu(c_h)\boldsymbol{\varepsilon}_h(\boldsymbol{u}_h)\}\!\} : [\![\boldsymbol{v}_h]\!] - \{\!\{\nu(c_h)\boldsymbol{\varepsilon}_h(\boldsymbol{v}_h)\}\!\} : [\![\boldsymbol{u}_h]\!] + \frac{a_0}{h_e}\nu(c_h)[\![\boldsymbol{u}_h]\!] : [\![\boldsymbol{v}_h]\!]\Big),
\end{aligned}$$

$$c_1^h(\boldsymbol{w}_h; \boldsymbol{u}_h, \boldsymbol{v}_h) := \int_\Omega (\boldsymbol{w}_h \cdot \nabla)\boldsymbol{u}_h \cdot \boldsymbol{v}_h + \sum_{K \in \mathcal{T}_h} \int_{\partial K \backslash \Gamma} \hat{\boldsymbol{w}}_h^{\mathrm{up}}(\boldsymbol{u}_h) \cdot \boldsymbol{v}_h,$$

where the upwind flux is defined as $\hat{\boldsymbol{w}}_h^{\mathrm{up}}(\boldsymbol{u}_h) := \frac{1}{2}(\boldsymbol{w}_h \cdot \boldsymbol{n}_k - |\boldsymbol{w}_h \cdot \boldsymbol{n}_K|)(\boldsymbol{u}_h^e - \boldsymbol{u}_h)$, and $\boldsymbol{u}_h^e$ is the trace of $\boldsymbol{u}_h$ taken from within the exterior of K.

Let us introduce a partition of the interval $[0, T]$ into N subintervals $[t_{n-1}, t_n]$ of length τ. We will use an implicit, second-order backward differentiation formula (BDF2). That is, all first-order time derivatives are approximated using the centred operator

$$\partial_t \boldsymbol{u}_h(t^{n+1}) \approx \frac{1}{\tau}\left(\frac{3}{2}\boldsymbol{u}_h^{n+1} - 2\boldsymbol{u}_h^n + \frac{1}{2}\boldsymbol{u}_h^{n-1}\right)$$

(similarly for $\partial_t c$) whereas for the first time step (from t^0 to t^1) a first-order backward Euler method is used, starting from the interpolates $\boldsymbol{u}_h^0$ and c_h^0 of the initial data. The resulting set of nonlinear equations is solved with an iterative Newton–Raphson method with exact Jacobian.

3.2. Spatio-temporal accuracy of the discretisation

For sake of the subsequent analysis, we assume Lipschitz continuity of the concentration-dependent viscosity

$$\nu \in \mathrm{Lip}(\mathbb{R}_+); \quad \exists \nu_{\min} > 0, \nu_{\max} > 0 : \forall c \in \mathbb{R}_+ : \nu_{\min} \le \nu(c) \le \nu_{\max}.$$

Moreover, the flux $f_{\mathrm{bk}}(c)$ is assumed to be Lipschitz continuous, and the diffusion coefficient $D = D(c)$ is supposed to be a nonlinear function satisfying

$$D \in \mathrm{Lip}(\mathbb{R}_+); \quad \exists D_1 > 0, D_2 > 0 : \forall c \in \mathbb{R}_+ : D_1 \le D(c) \le D_2. \tag{3.10}$$

For simplicity, we impose the following modified boundary conditions:

$$\boldsymbol{u}(\boldsymbol{x}, t) = \boldsymbol{0}, \quad c(\boldsymbol{x}, t) = 0, \quad \big(D(c)\nabla c - f_{\mathrm{bk}}(c)\boldsymbol{k}\big) \cdot \boldsymbol{n} = 0 \quad \text{on } \Gamma, t \in [0, T],$$

and we emphasise that the analysis can be extended to the non-homogeneous case following, for instance, lifting arguments.

We utilise the following mesh dependent broken norms:

$$\|\boldsymbol{v}\|_{*, \mathcal{T}_h}^2 := \sum_{K \in \mathcal{T}_h} \|\nabla \boldsymbol{v}\|_{0,K}^2 + \sum_{e \in \mathcal{E}_h} \frac{1}{h_e}\|[\![\boldsymbol{v}]\!]\|_{0,e}^2, \quad \|\boldsymbol{v}\|_{1, \mathcal{T}_h}^2 := \|\boldsymbol{v}\|_{0, \Omega}^2 + \|\boldsymbol{v}\|_{*, \mathcal{T}_h}^2 \quad \text{for all } \boldsymbol{v} \in \mathbf{H}^1(\mathcal{T}_h),$$

$$\|\boldsymbol{v}\|_{2, \mathcal{T}_h}^2 := \|\boldsymbol{v}\|_{1, \mathcal{T}_h}^2 + \sum_{K \in \mathcal{T}_h} h_K^2 |\boldsymbol{v}|_{2,K}^2 \quad \text{for all } \boldsymbol{v} \in \mathbf{H}^2(\mathcal{T}_h).$$

We also recall the broken version of the well-known Sobolev embedding result (see e.g. [29, Lemma 6.2], [30, Prop. 4.5] or [31, Th. 5.3]): for any $r > 1$ if $d = 2$ or $1 \le r \le 6$ if $d = 3$ there exists a constant $C_{\mathrm{emb}} > 0$ such that

$$\|\boldsymbol{v}\|_{\mathbf{L}^r(\Omega)} \le C_{\mathrm{emb}}\|\boldsymbol{v}\|_{1, \mathcal{T}_h} \quad \text{for all } \boldsymbol{v} \in \mathbf{H}^1(\mathcal{T}_h). \tag{3.11}$$

Furthermore, we will use the broken space

$$\mathbf{C}^1(\mathcal{T}_h) := \big\{\boldsymbol{u} \in \mathbf{H}^1(\mathcal{T}_h) : \boldsymbol{u}|_K \in \mathbf{C}^1(\bar{K}), K \in \mathcal{T}_h\big\},$$

equipped with an appropriate norm $\|\boldsymbol{u}\|_{\mathbf{W}^{1,\infty}(\mathcal{T}_h)} := \max_{K \in \mathcal{T}_h} \|\boldsymbol{u}\|_{\mathbf{W}^{1,\infty}(K)}$. Using the discrete norms, embedding (3.11) and local trace inequalities, we can establish continuity of the trilinear and bilinear forms involved, stated in the following lemma that can be proved following [28, Section 4]:

Lemma 3.1. *The following properties hold:*

$$\big|a_1^h(\cdot, \boldsymbol{u}, \boldsymbol{v})\big| \le \tilde{C}_a\|\boldsymbol{u}\|_{1, \mathcal{T}_h}\|\boldsymbol{v}\|_{1, \mathcal{T}_h} \quad \text{for all } \boldsymbol{u}, \boldsymbol{v} \in \mathbf{V}_h, \tag{3.12a}$$

$$\big|b(\boldsymbol{v}, q)\big| \le \|\boldsymbol{v}\|_{1, \mathcal{T}_h}\|q\|_{0, \Omega} \quad \text{for all } \boldsymbol{v} \in \mathbf{H}^1(\mathcal{T}_h), q \in L_0^2(\Omega), \tag{3.12b}$$

$$\big|c_2(\boldsymbol{w}; c, l)\big| \le \tilde{C}_1\|\boldsymbol{w}\|_{1, \mathcal{T}_h}\|l\|_{1, \Omega}\|c\|_{1, \Omega} \quad \text{for all } \boldsymbol{w} \in \mathbf{H}^1(\mathcal{T}_h) \text{ and } l, c \in H^1(\Omega). \tag{3.12c}$$

Moreover, for $c_1, c_2 \in H^1(\Omega)$, $c \in W^{1,\infty}(\Omega)$, $\boldsymbol{u} \in \mathbf{C}^1(\mathcal{T}_h) \cap \mathbf{H}_0^1(\Omega)$ and $\boldsymbol{v} \in \mathbf{V}_h$, there hold

$$\left| a_1^h(c_1; \boldsymbol{u}, \boldsymbol{v}) - a_1^h(c_2; \boldsymbol{u}, \boldsymbol{v}) \right| \leq \tilde{C}_{\mathrm{Lip}} \|c_1 - c_2\|_{1,\Omega} \|\boldsymbol{u}\|_{\mathbf{W}^{1,\infty}(\mathcal{T}_h)} \|\boldsymbol{v}\|_{1,\mathcal{T}_h},$$
$$\left| a_2(c_1, c, l) - a_2(c_2, c, l) \right| \leq \hat{C}_{\mathrm{Lip}} \|c_1 - c_2\|_{1,\Omega} \|c\|_{W^{1,\infty}(\Omega)} \|l\|_{1,\Omega}, \tag{3.13}$$

where the constant $\tilde{C}_{\mathrm{Lip}} > 0$ is independent of h (cf. [4]). A related result follows for $c_1^h(\cdot; \cdot, \cdot)$ as in [32, Lemma 3.4]. On the other hand, let $\boldsymbol{w}_1, \boldsymbol{w}_2, \boldsymbol{u} \in \mathbf{H}^2(\mathcal{T}_h)$ and $\boldsymbol{v} \in V_h$. Then there exists $\tilde{C}_u > 0$ independently of h such that

$$\left| c_1^h(\boldsymbol{w}_1; \boldsymbol{u}, \boldsymbol{v}) - c_1^h(\boldsymbol{w}_2; \boldsymbol{u}, \boldsymbol{v}) \right| \leq \tilde{C}_u \|\boldsymbol{w}_1 - \boldsymbol{w}_2\|_{1,\mathcal{T}_h} \|\boldsymbol{u}\|_{1,\mathcal{T}_h} \|\boldsymbol{v}\|_{1,\mathcal{T}_h}. \tag{3.14}$$

Moreover, while the coercivity of the form $a_2(\cdot, \cdot, \cdot)$, that is

$$a_2(\cdot, c, c) \geq \hat{\alpha}_a \|c\|_{1,\Omega}^2 \quad \text{for all } c \in H^1(\Omega), \tag{3.15}$$

is readily implied by (3.10), there also holds (cf. [27, Lemma 3.2])

$$a_1^h(\cdot, \boldsymbol{v}, \boldsymbol{v}) \geq \tilde{\alpha}_a \|\boldsymbol{v}\|_{1,\mathcal{T}_h}^2 \quad \text{for all } \boldsymbol{v} \in \mathbf{V}_h, \tag{3.16}$$

provided that $a_0 > 0$ is sufficiently large and independent of the meshsize.

Furthermore, based on the assumptions on D, we have

$$\left| a_2(\cdot; c, l) \right| \leq \hat{C}_a \|c\|_{1,\Omega} \|l\|_{1,\Omega} \quad \text{for all } c, l \in H^1(\Omega). \tag{3.17}$$

In addition, if we let $\boldsymbol{w} \in \mathbf{H}_0(\mathrm{div}^0; \Omega) := \{\boldsymbol{w} \in \mathbf{H}(\mathrm{div}, \Omega) : \boldsymbol{w} \cdot \boldsymbol{n} = 0 \text{ on } \partial\Omega, \mathrm{div}\,\boldsymbol{w} = 0 \text{ in } \Omega\}$, then according to [32] we can write

$$c_1^h(\boldsymbol{w}; \boldsymbol{u}, \boldsymbol{u}) = \frac{1}{2} \sum_{e \in \mathcal{E}_h^i} \int_e |\boldsymbol{w} \cdot \boldsymbol{n}_e| [\![\boldsymbol{u}]\!]^2 \geq 0 \quad \text{for all } \boldsymbol{u} \in \mathbf{V}_h, \tag{3.18}$$

as well as the relation

$$c_2(\boldsymbol{w}; l_h, l_h) = 0 \quad \text{for all } l_h \in \mathcal{M}_h, \tag{3.19}$$

which arises from integration by parts and holds at the discrete level since the produced discrete velocities are exactly divergence free. Based on the assumptions on f_{bk}, it is also clear that

$$\left| d_2(c_1, l) - d_2(c_2, l) \right| \leq C_d \|c_1 - c_2\|_{0,\Omega} \|l\|_{1,\Omega}. \tag{3.20}$$

Finally, we recall from [27] the following discrete inf–sup condition for $b(\cdot, \cdot)$, where $\tilde{\beta}$ is independent of h:

$$\sup_{\boldsymbol{v}_h \in \mathbf{V}_h \setminus \{\mathbf{0}\}} \frac{b(\boldsymbol{v}_h, q_h)}{\|\boldsymbol{v}_h\|_{1,\mathcal{T}_h}} \geq \tilde{\beta} \|q_h\|_{0,\Omega} \quad \text{for all } q_h \in \mathcal{Q}_h. \tag{3.21}$$

Remark 3.1. Using the definition and characterisation of the kernel $\mathbf{Z}$ of $b(\cdot, \cdot)$, namely

$$\mathbf{Z} := \left\{ \boldsymbol{v} \in \mathbf{H}_0^1(\Omega) : b(\boldsymbol{v}, q) = 0 \; \forall q \in L_0^2(\Omega) \right\} = \left\{ \boldsymbol{v} \in \mathbf{H}_0^1(\Omega) : \mathrm{div}\,\boldsymbol{v} = 0 \text{ in } \Omega \right\},$$

and using integration by parts, we can readily observe that

$$c_1(\boldsymbol{w}; \boldsymbol{v}, \boldsymbol{v}) = 0 \quad \text{and} \quad c_2(\boldsymbol{w}; s, s) = 0 \quad \text{for all } \boldsymbol{w} \in \mathbf{X}, \boldsymbol{v} \in \mathbf{H}^1(\Omega), \text{ and } s \in H^1(\Omega).$$

It is also well known (see for instance [33]) that if $(\boldsymbol{u}, p, c) \in \mathbf{H}_0^1(\Omega) \times L_0^2 \times H^1$ solves (2.8), then $\boldsymbol{u} \in \mathbf{Z}$ is a solution of the following reduced problem:

For all $t \in (0, T]$, find $(\boldsymbol{u}, c) \in \mathbf{Z} \times H^1$ such that

$$\left(\partial_t \boldsymbol{u}(t), \boldsymbol{v} \right)_\Omega + a_1\left(c(t); \boldsymbol{u}(t), \boldsymbol{v} \right) + c_1\left(\boldsymbol{u}(t); \boldsymbol{u}(t), \boldsymbol{v} \right) = \mathbf{F}_\mathrm{g}(c, \boldsymbol{v}) + \mathbf{F}_\mathrm{r}(\boldsymbol{u}, \boldsymbol{v}) \quad \text{for all } \boldsymbol{v} \in \mathbf{H}_0^1(\Omega),$$
$$\left(\partial_t c(t), l \right)_\Omega + a_2\left(c(t); c(t), l \right) + c_2\left(\boldsymbol{u}(t); c(t), l \right) - d_2\left(c(t), l \right) = -G_\mathrm{r}(c(t), l) \quad \text{for all } l \in H^1(\Omega). \tag{3.22}$$

Conversely, if $(\boldsymbol{u}, c) \in \mathbf{Z} \times H^1$ is a solution of (3.22), then there exists a pressure $p \in L_0^2$ such that $(\boldsymbol{u}, p, c)$ is a solution of (2.8). As in the continuous case, we define the discrete kernel of the bilinear form $b(\cdot, \cdot)$ as

$$\mathbf{Z}_h := \left\{ \boldsymbol{v}_h \in \mathbf{V}_h : b(\boldsymbol{v}_h, q_h) = 0 \; \forall q_h \in \mathcal{Q}_h \right\} = \left\{ \boldsymbol{v}_h \in \mathbf{V}_h : \mathrm{div}\,\boldsymbol{v}_h = 0 \text{ in } \Omega \right\},$$

and relying on the inf–sup condition (3.21), we can introduce an equivalent discrete reduce problem.

Let us denote by $\mathcal{I}_h : C(\bar{\Omega}) \to \mathcal{M}_h$ the classical nodal interpolation operator with respect to a unisolvent set of Lagrangian interpolation nodes associated with the conforming space $\mathcal{M}_h$. By $\Pi_h \boldsymbol{u}$ we denote the BDM projection of $\boldsymbol{u}$, and $\mathcal{L}_h p$ is the L^2-projection of p onto $\mathcal{Q}_h$. Under adequate regularity assumptions, the following approximation properties hold (see [27]):

$$\begin{aligned}
&\|\boldsymbol{u} - \Pi_h \boldsymbol{u}\|_{1,\mathcal{T}_h} \leq C^* h^{k+1} \|\boldsymbol{u}\|_{k+1,\Omega}, \\
&\|c - \mathcal{I}_h c\|_{1,\Omega} \leq C^* h^k \|c\|_{k+1,\Omega}, \quad \|p - \mathcal{L}_h p\|_{0,\Omega} \leq C^* h^k \|p\|_{k,\Omega}.
\end{aligned} \tag{3.23}$$

The following development follows the structure adopted in [34].

Lemma 3.2. *Assume that $\boldsymbol{u} \in \mathbf{H}^2(\Omega)$, $p \in L^2(\Omega)$ and $c \in H^1(\Omega)$. Then we have*

For all $\boldsymbol{v} \in \mathbf{V}_h$, $q \in \mathcal{Q}_h$ and $l \in \mathcal{M}_h$:

$$\left(\partial_t \boldsymbol{u}(t), \boldsymbol{v}\right)_\Omega + a_1^h\big(c(t); \boldsymbol{u}(t), \boldsymbol{v}\big) + c_1^h\big(\boldsymbol{u}(t); \boldsymbol{u}(t), \boldsymbol{v}\big) - b(\boldsymbol{v}, p(t)) - \mathbf{F}_g\big(c(t), \boldsymbol{v}\big) - \mathbf{F}_r\big(\boldsymbol{u}(t), \boldsymbol{v}\big) = 0,$$
$$b(\boldsymbol{u}(t), q) = 0,$$
$$\left(\partial_t c(t), l\right)_\Omega + a_2\big(c(t); c(t), l\big) + c_2\big(\boldsymbol{u}(t); c(t), l\big) - d_2\big(c(t), l\big) = -G_r\big(c(t), l\big).$$

Proof. Since we assume $\boldsymbol{u} \in \mathbf{H}^2(\Omega)$, integration by parts yields the required result. See also [28]. The third equation is a straightforward consequence of the continuous form. $\square$

Now we decompose the errors as follows:

$$\begin{aligned}
\boldsymbol{u}_h - \boldsymbol{u} &= E_{\boldsymbol{u}} + \xi_{\boldsymbol{u}} = (\Pi_h \boldsymbol{u} - \boldsymbol{u}) + (\boldsymbol{u}_h - \Pi_h \boldsymbol{u}), \\
p_h - p &= E_p + \xi_p = (\mathcal{L}_h p - p) + (p_h - \mathcal{L}_h p), \\
c_h - c &= E_c + \xi_c = (\mathcal{I}_h c - c) + (c_h - \mathcal{I}_h c).
\end{aligned}$$

Assuming that $\boldsymbol{u}_h^0 = \Pi_h \boldsymbol{u}(0)$ and $c_h^0 = \mathcal{I}_h c(0)$, we also use the notation $E_{\boldsymbol{u}}^n = (\boldsymbol{u}(t_n) - \Pi_h \boldsymbol{u}(t_n))$ and $\xi_{\boldsymbol{u}}^n = (\Pi_h \boldsymbol{u}(t_n) - \boldsymbol{u}_h^n)$, and similar notation for other variables. Note that for the first time iteration of the fully discrete form of system (3.9) we adopt a backward Euler scheme, and so we require error estimates for this step.

In what follows we assume a simpler form for the drag term $\boldsymbol{f}_r$ such that for all $\boldsymbol{u}_1, \boldsymbol{u}_2, \boldsymbol{v} \in \mathbf{H}^1(\Omega)$ we have the following Lipschitz continuity:

$$\left|\mathbf{F}_r(\boldsymbol{u}_1, \boldsymbol{v}) - \mathbf{F}_r(\boldsymbol{u}_2, \boldsymbol{v})\right| \leq \tilde{\gamma}_1 \|\boldsymbol{u}_1 - \boldsymbol{u}_2\|_{0,\mathcal{B}} \|\boldsymbol{v}\|_{0,\mathcal{B}}. \tag{3.24}$$

Since $\mathbf{X}_r(\boldsymbol{s}, t)$ is a rigid motion, (3.24) can be achieved, for instance, if we consider

$$\boldsymbol{f}_r(\boldsymbol{x}, t) = \beta^* \rho_r \int_\mathcal{B} \big((\boldsymbol{u}_r(\boldsymbol{s}) - \boldsymbol{u}(\mathbf{X}_r(\boldsymbol{s}, t), t)) \cdot \boldsymbol{n}_r\big) \boldsymbol{n}_r \delta(\boldsymbol{x} - \mathbf{X}_r(\boldsymbol{s}, t)) \, \mathrm{d}\boldsymbol{s}. \tag{3.25}$$

Furthermore, since $\mathcal{B} \subset \Omega$, we have that $\|\cdot\|_{0,\mathcal{B}} \leq \|\cdot\|_{0,\Omega}$ and

$$\left|\mathbf{F}_r(\boldsymbol{u}_1, \boldsymbol{v}) - \mathbf{F}_r(\boldsymbol{u}_2, \boldsymbol{v})\right| \leq \gamma_1 \|\boldsymbol{u}_1 - \boldsymbol{u}_2\|_{0,\Omega} \|\boldsymbol{v}\|_{0,\Omega}. \tag{3.26}$$

By Hölder's inequality for all $c, c_1, c_2, l \in H^1(\Omega)$ and $\boldsymbol{v} \in \mathbf{H}^1(\Omega)$ there also hold

$$\mathbf{F}_g(c, \boldsymbol{v}) \leq \gamma_2 \|c\|_{0,\Omega} \|\boldsymbol{v}\|_{0,\Omega}, \tag{3.27}$$
$$G_r(c_1, l) - G_r(c_2, l) \leq \gamma_3 \|c_1 - c_2\|_{0,\Omega} \|l\|_{0,\Omega}. \tag{3.28}$$

The following algebraic relation will be useful in the sequel: for any real numbers a^{n+1}, a^n, a^{n-1} and defining $\Lambda a^n := a^{n+1} - 2a^n + a^{n-1}$, we have

$$2(3a^{n+1} - 4a^n + a^{n-1}, a^n) = |a^{n+1}|^2 + |2a^{n+1} - a^n|^2 + |\Lambda a^n|^2 - |a^n|^2 - |2a^n - a^{n-1}|^2. \tag{3.29}$$

Theorem 3.1. *Let $(\boldsymbol{u}_h^n, c_h^n)$ in $\mathbf{X}_h \times \mathcal{M}_h$ be a solution of problem (3.9) based on the second-order backward differentiation formula (BDF2) with initial data $(\boldsymbol{u}_h^1, c_h^1)$ and $(\boldsymbol{u}_h^0, c_h^0)$. Then there exist constants $\bar{C}_u > 0$ and $\bar{C}_c > 0$ that are independent of h and τ such that*

$$\sup_{2 \leq n \leq N} \|\boldsymbol{u}_h^n\|_{0,\Omega}^2 + \sup_{2 \leq n \leq N} \|2\boldsymbol{u}_h^n - \boldsymbol{u}_h^{n-1}\|_{0,\Omega}^2 + \sum_{n=2}^N \|\Lambda \boldsymbol{u}_h^{n-1}\|_{0,\Omega} + \sum_{n=2}^N \tau \tilde{\alpha}_a \|\boldsymbol{u}_h^n\|_{1,\mathcal{T}_h}^2$$

$$\leq \bar{C}_{\boldsymbol{u}}(\|c_h^1\|_{0,\Omega}^2 + \|2c_h^1 - c_h^0\|_{0,\Omega}^2 + \|\boldsymbol{u}_h^1\|_{0,\Omega}^2 + \|2\boldsymbol{u}_h^1 - \boldsymbol{u}_h^0\|_{0,\Omega}^2 + \|\boldsymbol{u}_r\|_{0,\mathcal{B}}^2 + |c_r|^2),$$

$$\sup_{2\leq n\leq N} \|c_h^n\|_{0,\Omega}^2 + \sup_{2\leq n\leq N} \|2c_h^n - c_h^{n-1}\|_{0,\Omega}^2 + \sum_{n=2}^{N} \|\Lambda c_h^{n-1}\|_{0,\Omega} + 4\sum_{n=2}^{N} \tau\hat{\alpha}_a\|c_h^n\|_{1,\Omega}^2$$

$$\leq \bar{C}_c(\|c_h^1\|_{0,\Omega}^2 + \|2c_h^1 - c_h^0\|_{0,\Omega}^2 + |c_r|^2).$$

Proof. It suffices to take $\boldsymbol{v}_h = 4\tau\boldsymbol{u}_h^{n+1}$ and $l_h = 4\tau c_h^{n+1}$ in system (3.9), using BDF2 differentiation formula, Sobolev inequalities, summing over n from 1 to $n \leq N - 1$, and applying Gronwall's lemma, with τ sufficiently small. Note that by Remark 3.1, all terms containing the bilinear form b are simply removed from the system. □

Theorem 3.2. *Let us assume that* $\boldsymbol{u} \in L^\infty(0, T; \mathbf{H}_0^{k+1}(\Omega))$, $\boldsymbol{u}' \in L^\infty(0, T; \mathbf{H}^1(\Omega))$, $\boldsymbol{u}'' \in L^\infty(0, T; \mathbf{L}^2(\Omega))$, $p \in L^\infty(0, T; H^k(\Omega))$, $c \in L^\infty(0, T; H_0^{k+1}(\Omega))$, $c' \in L^\infty(0, T; H^k(\Omega))$, $c'' \in L^\infty(0, T; L^2(\Omega))$, *with* $\gamma_2^2 \leq \frac{1}{32}\hat{\alpha}_a\tilde{\alpha}_a$, $k \geq 1$ *and also that*

$$\max\{\|\boldsymbol{u}\|_{L^\infty(0,T;\mathbf{W}^{1,\infty}(\Omega))}, \|c\|_{L^\infty(0,T;W^{1,\infty}(\Omega))}\} < M,$$

for a sufficiently small constant $M > 0$ *(a precise condition on* M *can be found in* Theorem 3.5*). Then there exist positive constants* C_u^1, C_c^1, *independent of* h *and* τ, *such that*

$$\frac{1}{4}\|\xi_{\boldsymbol{u}}^1\|_{0,\Omega}^2 + \frac{1}{4}\tau\tilde{\alpha}_a\|\xi_{\boldsymbol{u}}^1\|_{1,\mathcal{T}_h}^2 \leq C_u^1(h^{2k} + \tau^4), \quad \frac{1}{8}\|\xi_c^1\|_{0,\Omega}^2 + \frac{1}{4}\tau\hat{\alpha}_a\|\xi_c^1\|_{H^1(\Omega)}^2 \leq C_c^1(h^{2k} + \tau^4).$$

Proof. First, taking into account the regularity assumptions for $\boldsymbol{u}$, we have that for all $\boldsymbol{x}$ there exists $\gamma \in (0, 1)$ that depends on $\boldsymbol{x}$ such that

$$\boldsymbol{u}(0) = \boldsymbol{u}(\tau) - \tau\boldsymbol{u}'(\tau) + \frac{1}{2}\tau^2\boldsymbol{u}''(\tau\gamma).$$

Then, using the reduced problem as stated in Remark 3.1, we deduce that $\boldsymbol{u}$ satisfies the following error estimate:

$$\|\xi_{\boldsymbol{u}}^1\|_{0,\Omega}^2 + \tau\tilde{\alpha}_a\|\xi_{\boldsymbol{u}}^1\|_{1,\mathcal{T}_h}^2 \leq -\big(\Pi_h\boldsymbol{u}(\tau) - \boldsymbol{u}(\tau) + \boldsymbol{u}_h^0 - \boldsymbol{u}(0), \xi_{\boldsymbol{u}}^1\big)_\Omega$$
$$+ \tau\big(a_1^h(c_h^1; \Pi_h\boldsymbol{u}(\tau), \xi_{\boldsymbol{u}}^1) - a_1^h(c^1; \boldsymbol{u}(\tau), \xi_{\boldsymbol{u}}^1)\big)$$
$$- \tau\big(c_1^h(\boldsymbol{u}_h^1; \boldsymbol{u}_h^1, \xi_{\boldsymbol{u}}^1) - c_1^h(\boldsymbol{u}(\tau), \boldsymbol{u}(\tau), \xi_{\boldsymbol{u}}^1)\big) - \tau\big(\mathbf{F}_r(\boldsymbol{u}_h^1, \xi_{\boldsymbol{u}}^1) - \mathbf{F}_r(\boldsymbol{u}(\tau), \xi_{\boldsymbol{u}}^1)\big)$$
$$- \tau\big(\mathbf{F}_g(c_h^1, \xi_{\boldsymbol{u}}^1) - \mathbf{F}_g(c(\tau), \xi_{\boldsymbol{u}}^1)\big) - \frac{\tau^2}{2}\big(\boldsymbol{u}''(\tau\gamma), \xi_{\boldsymbol{u}}^1\big),$$

which results after choosing $\xi_{\boldsymbol{u}}^1$ as test function in the first equation of Lemma 3.2 and system (3.9), performing an Euler scheme step, subtracting both equations, and adding $\pm a_1^h(c_h^1; \Pi_h\boldsymbol{u}(\tau), \xi_{\boldsymbol{u}}^1)$. Now, by applying the error estimates (3.23), Young's inequality, and the stability properties, we get

$$\frac{1}{4}\|\xi_{\boldsymbol{u}}^1\|_{0,\Omega}^2 + \frac{1}{4}\tau\tilde{\alpha}_a\|\xi_{\boldsymbol{u}}^1\|_{1,\mathcal{T}_h}^2 \leq Ch^{2k}\tau\Big(\|\boldsymbol{u}(\tau)\|_{\mathbf{H}^{k+1}(\Omega)}^2 + \|\boldsymbol{u}(0)\|_{\mathbf{H}^{k+1}(\Omega)}^2 + \|c(\tau)\|_{H^{k+1}(\Omega)}^2 + \|p(\tau)\|_{H^k(\Omega)}^2\Big)$$
$$+ C\tau^4(\|\boldsymbol{u}''\|_{L^\infty(0,T;\mathbf{L}^2(\Omega))}^2) + \frac{4\tilde{C}_{\text{Lip}}^2 M^2}{\tilde{\alpha}_a}\tau\|\xi_c^1\|_{1,\Omega}^2 + \tau\frac{\gamma_2^2}{\tilde{\alpha}_a}\|\xi_c^1\|_{1,\Omega}^2. \tag{3.30}$$

Next we follow the same steps for c, with τ sufficiently small ($\tau \leq \frac{1}{2(12C_d^2 + 2\tilde{\gamma}_3^2)}$), to obtain

$$\frac{1}{4}\|\xi_c^1\|_{0,\Omega}^2 + \frac{1}{2}\tau\hat{\alpha}_a\|\xi_c^1\|_{1,\Omega}^2 \leq C\tau h^{2k}\Big(\|\boldsymbol{u}(\tau)\|_{\mathbf{H}^{k+1}(\Omega)}^2 + \|c(\tau)\|_{H^{k+1}(\Omega)}^2 + \|c(0)\|_{H^{k+1}(\Omega)}^2$$
$$+ \|c(\tau)\|_{H^{k+1}(\Omega)}^2\|\boldsymbol{u}(\tau)\|_{H^1(\Omega)}^2 + \|\boldsymbol{u}(\tau)\|_{H^{k+1}(\Omega)}^2\|c(\tau)\|_{H^1(\Omega)}^2\Big) \tag{3.31}$$
$$+ C\tau^4(\|c''\|_{L^\infty(0,\tau;L^2(\Omega))}^2) + \frac{6\tilde{C}_1^2(1 + C^*)^2 M^2}{\hat{\alpha}_a}\tau\|\xi_{\boldsymbol{u}}^1\|_{1,\mathcal{T}_h}^2.$$

In this way, from (3.30) we deduce that

$$\tau\|\xi_{\boldsymbol{u}}^1\|_{1,\mathcal{T}_h}^2 \leq C(h^{2k} + \tau^4) + \frac{16\tilde{C}_{\text{Lip}}^2 M^2}{\tilde{\alpha}_a^2}\tau\|\xi_c^1\|_{1,\Omega}^2 + 4\frac{\gamma_2^2}{\tilde{\alpha}_a^2}\tau\|\xi_c^1\|_{1,\Omega}^2.$$

We insert the previous inequality into (3.31) and consider M sufficiently small such that the terms multiplying $\|\xi_c\|_{1,\Omega}^2$ can be absorbed into the left-hand side of the inequality to get

$$\frac{1}{8}\|\xi_c^1\|_{0,\Omega}^2 + \frac{1}{4}\tau\hat{\alpha}_a\|\xi_c\|_{1,\Omega}^2 \leq C_c^1(h^{2k} + \tau^4). \tag{3.32}$$

The first estimate follows by directly substituting (3.32) into (3.30). $\square$

Theorem 3.3. *Let $(\boldsymbol{u}, p, c)$ be the solution of (2.8) and $(\boldsymbol{u}_h, p_h, c_h)$ be the solution of (3.9) with BDF2 iteration. Suppose that $\boldsymbol{u} \in L^\infty(0, T; \mathbf{H}_0^{k+1}(\Omega))$, $c \in L^\infty(0, T; H_0^{k+1}(\Omega))$, $\boldsymbol{u}' \in L^\infty(0, T; \mathbf{H}^k(\Omega))$, $\boldsymbol{u}^{(3)} \in L^2(0, T; \mathbf{L}^2(\Omega))$ and $\|\boldsymbol{u}\|_{L^\infty(0,T;\mathbf{W}^{1,\infty}(\Omega))} < M$ for a sufficiently small constant $M > 0$. Then there exist constants $C, \eta_1 \geq 0$ independent of h and τ such that for all $m + 1 \leq N$,*

$$\|\xi_{\boldsymbol{u}}^{m+1}\|_{0,\Omega}^2 + \|2\xi_{\boldsymbol{u}}^{m+1} - \xi_{\boldsymbol{u}}^m\|_{0,\Omega}^2 + \sum_{n=1}^m \|\Lambda\xi_{\boldsymbol{u}}^n\|_{0,\Omega}^2 + \sum_{n=1}^m \tau\tilde{\alpha}_a\|\xi_{\boldsymbol{u}}^{n+1}\|_{1,\mathcal{T}_h}^2 \leq C(\tau^4 + h^{2k}) + \sum_{n=1}^m \eta_1\tau\|\xi_c^{n+1}\|_{0,\Omega}^2.$$

Proof. We choose as tests functions $\boldsymbol{v}_h = \xi_{\boldsymbol{u}}^{n+1}$ in the first equation of (3.9). Using BDF2 differentiation formula and inserting the terms

$$\pm\frac{1}{2\tau}\left(3\boldsymbol{u}(t_{n+1}) - 4\boldsymbol{u}(t_n) + \boldsymbol{u}(t_{n-1}), \xi_{\boldsymbol{u}}^{n+1}\right)_\Omega, \quad \pm\frac{1}{2\tau}\left(3\Pi_h\boldsymbol{u}(t_{n+1}) - 4\Pi_h\boldsymbol{u}(t_n) + \Pi_h\boldsymbol{u}(t_{n-1}), \xi_{\boldsymbol{u}}^{n+1}\right)_\Omega,$$

and $\pm a_1^h(c_h^{n+1}; \Pi_h\boldsymbol{u}(t_{n+1}), \xi_{\boldsymbol{u}}^{n+1})$, we get

$$\frac{1}{2\tau}\left(3\xi_{\boldsymbol{u}}^{n+1} - 4\xi_{\boldsymbol{u}}^n + \xi_{\boldsymbol{u}}^{n-1}, \xi_{\boldsymbol{u}}^{n+1}\right)_\Omega + \frac{1}{2\tau}\left(3E_{\boldsymbol{u}}^{n+1} - 4E_{\boldsymbol{u}}^n + E_{\boldsymbol{u}}^{n-1}, \xi_{\boldsymbol{u}}^{n+1}\right)_\Omega$$
$$+ \frac{1}{2\tau}\left(3\boldsymbol{u}(t_{n+1}) - 4\boldsymbol{u}(t_n) + \boldsymbol{u}(t_{n-1}), \xi_{\boldsymbol{u}}^{n+1}\right)_\Omega + a_1^h(c_h^{n+1}; \xi_{\boldsymbol{u}}^{n+1}, \xi_{\boldsymbol{u}}^{n+1}) + a_1^h(c_h^{n+1}; \Pi_h\boldsymbol{u}(t_{n+1}), \xi_{\boldsymbol{u}}^{n+1})$$
$$+ c_1^h(\boldsymbol{u}_h^{n+1}, \boldsymbol{u}_h^{n+1}, \xi_{\boldsymbol{u}}^{n+1}) = \mathbf{F}_g(c_h^{n+1}, \xi_{\boldsymbol{u}}^{n+1}) + \mathbf{F}_r(\boldsymbol{u}_h^{n+1}, \xi_{\boldsymbol{u}}^{n+1}). \tag{3.33}$$

Considering Lemma 3.2 at $t = t_{n+1}$ with $\boldsymbol{v} = \xi_{\boldsymbol{u}}^{n+1}$, and after inserting the term

$$\pm\frac{1}{2\tau}\left(3\boldsymbol{u}(t_{n+1}) - 4\boldsymbol{u}(t_n) + \boldsymbol{u}(t_{n-1}), \xi_{\boldsymbol{u}}^{n+1}\right)_\Omega,$$

we readily deduce the expression

$$\frac{1}{2\tau}\left(3\boldsymbol{u}(t_{n+1}) - 4\boldsymbol{u}(t_n) + \boldsymbol{u}(t_{n-1}), \xi_{\boldsymbol{u}}^{n+1}\right)_\Omega + a_1^h(c(t_{n+1}); \boldsymbol{u}(t_{n+1}), \xi_{\boldsymbol{u}}^{n+1}) + c_1^h(\boldsymbol{u}(t_{n+1}), \boldsymbol{u}(t_{n+1}), \xi_{\boldsymbol{u}}^{n+1})$$
$$= \mathbf{F}_g(c^{n+1}, \xi_{\boldsymbol{u}}^{n+1}) + \mathbf{F}_r(\boldsymbol{u}^{n+1}, \xi_{\boldsymbol{u}}^{n+1}) - \left(\boldsymbol{u}'(t_{n+1}) - \frac{3\boldsymbol{u}(t_{n+1}) - 4\boldsymbol{u}(t_n) + \boldsymbol{u}(t_{n-1})}{2\tau}, \xi_{\boldsymbol{u}}^{n+1}\right)_\Omega. \tag{3.34}$$

We can then subtract (3.33) from (3.34) and multiply both sides by 4τ to obtain an equality

$$I_1 + I_2 = I_3 + I_4 + I_5 + I_6 + I_7 + I_8,$$

where we define

$$I_1 := 2\left(3\xi_{\boldsymbol{u}}^{n+1} - 4\xi_{\boldsymbol{u}}^n + \xi_{\boldsymbol{u}}^{n-1}, \xi_{\boldsymbol{u}}^{n+1}\right)_\Omega, \quad I_2 := 4\tau a_1^h(c_h^{n+1}; \xi_{\boldsymbol{u}}^{n+1}, \xi_{\boldsymbol{u}}^{n+1}),$$
$$I_3 := 4\tau\left(\boldsymbol{u}'(t_{n+1}) - \frac{3\boldsymbol{u}(t_{n+1}) - 4\boldsymbol{u}(t_n) + \boldsymbol{u}(t_{n-1})}{2\tau}, \xi_{\boldsymbol{u}}^{n+1}\right)_\Omega, \quad I_4 := -2\left(3E_{\boldsymbol{u}}^{n+1} - 4E_{\boldsymbol{u}}^n + E_{\boldsymbol{u}}^{n-1}, \xi_{\boldsymbol{u}}^{n+1}\right)_\Omega,$$
$$I_5 := 4\tau\left(\mathbf{F}_g(c_h^{n+1}, \xi_{\boldsymbol{u}}^{n+1}) - \mathbf{F}_g(c(t_{n+1}), \xi_{\boldsymbol{u}}^{n+1})\right), \quad I_6 := 4\tau\left(\mathbf{F}_r(\boldsymbol{u}_h^{n+1}, \xi_{\boldsymbol{u}}^{n+1}) - \mathbf{F}_r(\boldsymbol{u}(t_{n+1}), \xi_{\boldsymbol{u}}^{n+1})\right),$$
$$I_7 := -4\tau\left(a_1^h(c_h^{n+1}; \Pi_h\boldsymbol{u}^{n+1}, \xi_{\boldsymbol{u}}^{n+1}) - a_1^h(c(t_{n+1}); \boldsymbol{u}(t_{n+1}), \xi_{\boldsymbol{u}}^{n+1})\right),$$
$$I_8 := -4\tau\left(c_1^h(\boldsymbol{u}_h^{n+1}, \boldsymbol{u}_h^{n+1}, \xi_{\boldsymbol{u}}^{n+1}) - c_1^h(\boldsymbol{u}(t_{n+1}), \boldsymbol{u}(t_{n+1}), \xi_{\boldsymbol{u}}^{n+1})\right).$$

Let us estimate each term I_i, $i \in \{1, \ldots, 8\}$. For I_1, using (3.29) we can assert that

$$I_1 = \|\xi_{\boldsymbol{u}}^{n+1}\|_{0,\Omega}^2 + \|2\xi_{\boldsymbol{u}}^{n+1} - \xi_{\boldsymbol{u}}^n\|_{0,\Omega}^2 + \|\Lambda\xi_{\boldsymbol{u}}^{n+1}\|_{0,\Omega}^2 - \|\xi_{\boldsymbol{u}}^n\|_{0,\Omega}^2 - \|2\xi_{\boldsymbol{u}}^n - \xi_{\boldsymbol{u}}^{n-1}\|_{0,\Omega}^2.$$

Using the ellipticity stated in (3.16), we readily get

$$I_2 \geq 4\tau \tilde{\alpha_a} \|\xi_u^{n+1}\|_{1,\mathcal{T}_h}^2.$$

By using Taylor's formula with integral remainder we have

$$\left| u'(t_{n+1}) - \frac{3u(t_{n+1}) - 4u(t_n) + u(t_{n-1})}{2\tau} \right| = \frac{\tau^{3/2}}{2\sqrt{3}} \|u^{(3)}\|_{L^2(t^{n-1}, t^{n+1}; \mathbf{L}^2(\Omega))},$$

then by combining Cauchy–Schwarz and Young's inequality, we obtain the bound

$$|I_3| \leq \frac{\tau^4}{24\varepsilon_1} \|u^{(3)}\|_{L^2(t_{n-1}, t_{n+1}; \mathbf{L}^2(\Omega))}^2 + \frac{\tau\varepsilon_1}{2} \|\xi_u^{n+1}\|_{1,\mathcal{T}_h}^2.$$

Now we insert $\pm 4\tau E_u'(t_{n+1})$ onto the fourth term, which leads to

$$I_4 = -4\tau(E_u'(t_{n+1}), \xi_u^{n+1})_\Omega + \left(E_u'(t_{n+1}) - \frac{3E_u^{n+1} - 4E_u^n + E_u^{n-1}}{2\tau}, \xi_u^{n+1} \right)_\Omega.$$

Proceeding as before and using (3.23) on the first term of I_4, we get

$$|I_4| \leq \frac{C}{2\varepsilon_2} h^{2k} \|u'\|_{\mathbf{L}^\infty(0,T;\mathbf{H}^k(\Omega))}^2 + \frac{\tau\varepsilon_2}{2} \|\xi_u^{n+1}\|_{1,\mathcal{T}_h}^2 + \frac{\tau^4 C}{2\varepsilon_3} \|u^{(3)}\|_{L^2(0,T;\mathbf{L}^2(\Omega))}^2 + \frac{\tau\varepsilon_3}{2} \|\xi_u^{n+1}\|_{1,\mathcal{T}_h}^2.$$

Now by (3.27), appealing to (3.23), and inserting $\pm 4\tau \mathbf{F}_g(\mathcal{I}_h c^{n+1}, \xi_u^{n+1})$, we are left with

$$|I_5| \leq \frac{2\gamma_2^2 \tau}{\varepsilon_4} \left(C^* h^{2k} \|c\|_{L^\infty(0,T;H^k(\Omega))}^2 + \|\xi_c^{n+1}\|_{0,\Omega}^2 \right) + 2\tau\varepsilon_4 \|\xi_u^{n+1}\|_{1,\mathcal{T}_h}^2.$$

In the same manner using (3.26), and inserting $\pm 4\tau \mathbf{F}_r(\Pi_h u^{n+1}, \xi_u^{n+1})$, we get

$$|I_6| \leq \frac{2\gamma_1^2 \tau}{\varepsilon_5} \left(C^* h^{2k} \|u\|_{L^\infty(0,T;\mathbf{H}^k(\Omega))}^2 + \|\xi_u\|_{0,\Omega}^2 \right) + 2\tau\varepsilon_5 \|\xi_u^{n+1}\|_{1,\mathcal{T}_h}^2$$

Again inserting $\pm a_1^h(c_h^{n+1}; u(t_{n+1}), \xi_u^{n+1})$ and $\pm a_1^h(\mathcal{I}_h c^{n+1}; u(t_{n+1}), \xi_u^{n+1})$ and using (3.23) we get

$$|I_7| \leq \frac{\tilde{C}_a^2 \tau h^{2k}}{2\varepsilon_6} \|u\|_{L^\infty(0,T;\mathbf{H}^{k+1}(\Omega))}^2 + \frac{\tau\varepsilon_6}{2} \|\xi_u^{n+1}\|_{1,\mathcal{T}_h}^2 + \frac{\tilde{C}_{\text{lip}}^2 M^2}{2\varepsilon_7} \|\xi_c\|_{1,\Omega}^2$$
$$+ \frac{\tau}{2}\varepsilon_7 \|\xi_u^{n+1}\|_{1,\mathcal{T}_h}^2 + \frac{\tilde{C}_{\text{lip}}^2 M^2 \tau h^{2k}}{2\varepsilon_8} \|c\|_{L^\infty(0,T;H^k(\Omega))}^2 + \frac{\varepsilon_8 \tau}{2} \|\xi_u^{n+1}\|_{1,\mathcal{T}_h}^2.$$

Now we insert into I_8 the three terms

$$\pm c_1^h(u(t_{n+1}), \Pi_h u(t_{n+1}), \xi_u^{n+1}), \quad \pm c_1^h(\Pi_h u(t_{n+1}), \Pi_h u(t_{n+1}), \xi_u^{n+1}),$$
$$\pm c_1^h(\Pi_h u(t_{n+1}), u(t_{n+1}), \xi_u^{n+1}),$$

which yields

$$I_8 = -4\tau \big(c_1^h(u(t_{n+1}), \Pi_h u(t_{n+1}), \xi_u^{n+1}) - c_1^h(\Pi_h u(t_{n+1}), \Pi_h u(t_{n+1}), \xi_u^{n+1})$$
$$+ c_1^h(\Pi_h u(t_{n+1}), \Pi_h u(t_{n+1}), \xi_u^{n+1}) - c_1^h(\Pi_h u(t_{n+1}), u(t_{n+1}), \xi_u^{n+1})$$
$$+ c_1^h(\Pi_h u(t_{n+1}), u(t_{n+1}), \xi_u^{n+1}) - c_1^h(u(t_{n+1})u(t_{n+1}), \xi_u^{n+1}) + c_1^h(u_h^{n+1}, \xi_u^{n+1}, \xi_u^{n+1}) \big).$$

The last term is moved to the left-hand side, where we use (3.18); whereas for the remaining terms (which we further rename as $\tilde{I}_8$), the bound (3.14) together with (3.23) imply that

$$|\tilde{I}_8| \leq 4\tau \bigg(C^* \tilde{C}_u C_\infty M \|\xi_u^{n+1}\|_{1,\mathcal{T}_h}^2 + \frac{h^{2k} C}{2\varepsilon_9} \|u\|_{L^\infty(0,T;\mathbf{H}^1(\Omega))}^2 \|u\|_{L^\infty(0,T;\mathbf{H}^{k+1}(\Omega))}^2 + \frac{\varepsilon_9}{2} \|\xi_u^{n+1}\|_{1,\mathcal{T}_h}^2$$
$$+ \frac{Ch^{2k}}{2\varepsilon_{10}} \|u\|_{L^\infty(0,T;\mathbf{H}^{k+1}(\Omega))}^2 \|u\|_{L^\infty(0,T;\mathbf{H}^1(\Omega))}^2 + \frac{\varepsilon_{10}}{2} \|\xi_u^{n+1}\|_{1,\mathcal{T}_h}^2 \bigg),$$

where C^* is a positive constant coming from (3.23). Hence, by choosing $\varepsilon_i = 2\tilde{\alpha}_a/11$ for $i = 1, \ldots, 11$, collecting the above estimates, and summing over $1 \leq n \leq m$ for all $m + 1 \leq N$ we get

$$\|\xi_{\boldsymbol{u}}^{m+1}\|_{0,\Omega}^2 + \|2\xi_{\boldsymbol{u}}^{m+1} - \xi_{\boldsymbol{u}}^m\|_{0,\Omega}^2 + \sum_{n=1}^m \|\Lambda\xi_{\boldsymbol{u}}^n\|_{0,\Omega}^2 - 3\|\xi_{\boldsymbol{u}}^1\|_{0,\Omega}^2 + \sum_{n=1}^m \tau\tilde{\alpha}_a\|\xi_{\boldsymbol{u}}^{n+1}\|_{1,\mathcal{T}_h}^2$$

$$\leq C(\tau^4 + h^{2k}) + \eta_1 \sum_{n=1}^m \|\xi_c^{n+1}\|_{0,\Omega}^2 + \sum_{n=1}^m \frac{11\gamma_1^2\tau}{\tilde{\alpha}_a}\|\xi_{\boldsymbol{u}}^{n+1}\|_{0,\Omega}^2,$$

where $\tilde{C}_u C^* C_\infty M \leq \tilde{\alpha}_a/4$ and $\eta_1 = C(\tilde{\alpha}_a, \tilde{C}_{\text{Lip}}, \gamma_1, \gamma_2)$. Finally, using Theorem 3.2, considering τ sufficiently small and applying Gronwall's lemma, we get the desired result. $\quad\square$

Theorem 3.4. *Let $(\boldsymbol{u}, c)$ be the solution of (2.8) and $(\boldsymbol{u}_h, c_h)$ be the solution of (3.9) using the BDF2 differential operator. If $\boldsymbol{u} \in L^\infty(0, T; \mathbf{H}_0^{k+1}(\Omega))$, $c \in L^\infty(0, T; H_0^{k+1}(\Omega))$, $c' \in L^\infty(0, T; H^k(\Omega))$, $c^{(3)} \in L^2(0, T; L^2(\Omega))$, and $\|c\|_{L^\infty(0,T;W^{1,\infty}(\Omega))} < M$; then there exist positive constants $C, \eta_2 > 0$, independent of h and τ, such that for all $m + 1 \leq N$*

$$\|\xi_c^{m+1}\|_{0,\Omega}^2 + \|2\xi_c^{m+1} - \xi_c^m\|_{0,\Omega}^2 + \sum_{n=1}^m \|\Lambda\xi_c^{n+1}\|_{0,\Omega}^2 + \sum_{n=1}^m \tau\hat{\alpha}_a\|\xi_c^{n+1}\|_{1,\Omega}^2$$

$$\leq C(\tau^4 + h^{2k}) + \sum_{n=1}^m \eta_2\tau\|\xi_{\boldsymbol{u}}^{n+1}\|_{1,\mathcal{T}_h}^2.$$

Proof. Proceeding similarly as in the proof of Theorem 3.3, from the second equation of (2.8) we get

$$
\begin{aligned}
&\frac{1}{2\tau}\left(3\xi_c^{n+1} - 4\xi_c^n + \xi_c^{n-1}, \xi_c^{n+1}\right)_\Omega + \frac{1}{2\tau}\left(3E_c^{n+1} - 4E_c^n + E_c^{n-1}, \xi_c^{n+1}\right)_\Omega \\
&+ \frac{1}{2\tau}\left(3c(t_{n+1}) - 4c(t_n) + c(t_{n-1}), \xi_c^{n+1}\right)_\Omega + a_2^h(\xi_c^{n+1}, \xi_c^{n+1}) + a_2^h(\mathcal{I}_h\, c(t_{n+1}), \xi_c^{n+1}) \\
&+ c_2^h(\boldsymbol{u}_h^{n+1}, c_h^{n+1}, \xi_c^{n+1}) - d_2(c_h^{n+1}, \xi_c^{n+1}) = -G_{\text{r}}(c_h^{n+1}, \xi_c^{n+1}),
\end{aligned}
\tag{3.35}
$$

and considering the third equation in Lemma 3.2, focusing on $t = t_{n+1}$, we immediately obtain

$$
\begin{aligned}
&\frac{1}{2\tau}\left(3c(t_{n+1}) - 4c(t_n) + c(t_{n-1}), \xi_c^{n+1}\right)_\Omega + a_2\left(c(t_{n+1}), \xi_c^{n+1}\right) + c_2\left(\boldsymbol{u}(t_{n+1}), c(t_{n+1}), \xi_c^{n+1}\right) \\
&- d_2(c^{n+1}, \xi_c^{n+1}) = -G_{\text{r}}(c^{n+1}, \xi_c^{n+1}) - \left(c'(t_{n+1}) - \frac{3c(t_{n+1}) - 4c(t_n) + c(t_{n-1})}{2\tau}, \xi_c^{n+1}\right)_\Omega.
\end{aligned}
\tag{3.36}
$$

Subtracting (3.35) from (3.36) and multiplying both sides of the result by 4τ leads to

$$
\begin{aligned}
&2\left(3\xi_c^{n+1} - 4\xi_c^n + \xi_c^{n-1}, \xi_c^{n+1}\right)_\Omega + 4\tau a_2(c_h^{n+1}; \xi_c^{n+1}, \xi_c^{n+1}) \\
&= 4\tau\left(c'(t_{n+1}) - \frac{3c(t_{n+1}) - 4c(t_n) + c(t_{n-1})}{2\tau}, \xi_c^{n+1}\right)_\Omega - 2\left(3E_c^{n+1} - 4E_c^n + E_c^{n-1}, \xi_c^{n+1}\right)_\Omega \\
&\quad - 4\tau\left(a_2(c_h^{n+1}; \mathcal{I}_h\, c^{n+1}, \xi_c^{n+1}) - a_2(c^{n+1}; c^{n+1}, \xi_c^{n+1})\right) \\
&\quad - 4\tau\left(c_2(\boldsymbol{u}_h^{n+1}, c_h^{n+1}, \xi_{\boldsymbol{u}}^{n+1}) - c_1^h(\boldsymbol{u}(t_{n+1}), c(t_{n+1}), \xi_{\boldsymbol{u}}^{n+1})\right) \\
&\quad + 4\tau\left(d_2(c_h^{n+1}, \xi_c^{n+1}) - d_2(c^{n1}, \xi_c^{n+1})\right) - 4\tau\left(G_{\text{r}}(c_h^{n+1}, \xi_c^{n+1}) - G_{\text{r}}(c^{n+1}, \xi_c^{n+1})\right).
\end{aligned}
\tag{3.37}
$$

As done above, we rewrite (3.37) using auxiliary terms now denoted $\hat{I}_1, \ldots, \hat{I}_8$, and derive individual bounds for each term. For the first, second, and third terms, we use (3.29), (3.15), and Taylor expansion together with Young's inequality, respectively, to obtain

$$\hat{I}_1 = \|\xi_c^{n+1}\|_{0,\Omega}^2 + \|2\xi_c^{n+1} - \xi_c^n\|_{0,\Omega}^2 + \|\Lambda\xi_c^{n+1}\|_{0,\Omega}^2 - \|\xi_c^n\|_{0,\Omega}^2 - \|2\xi_c^n - \xi_c^{n-1}\|_{0,\Omega}^2,$$

$$\hat{I}_2 \geq 4\tau\hat{\alpha}_a\|\xi_c^{n+1}\|_{1,\Omega}^2, \quad |\hat{I}_3| \leq \frac{\tau^4}{24\varepsilon_1}\|c^{(3)}\|_{L^2(t_{n-1},t_{n+1};L^2(\Omega))}^2 + \frac{\tau\varepsilon_1}{2}\|\xi_c^{n+1}\|_{1,\Omega}^2.$$

Now we insert $\pm 4\tau E'_c(t_{n+1})$ into $\hat{I}_4$ and exploit (3.23). This leads to the bound

$$|\hat{I}_4| \leq \frac{C}{2\varepsilon_2} h^{2k} \|c'\|^2_{L^\infty(0,T;H^k(\Omega))} + \frac{\tau\varepsilon_2}{2} \|\xi_c^{n+1}\|^2_{1,\Omega} + \frac{\tau^4 C}{2\varepsilon_3} \|c^{(3)}\|^2_{L^2(0,T;L^2(\Omega))} + \frac{\tau\varepsilon_3}{2} \|\xi_c^{n+1}\|^2_{1,\Omega}.$$

Employing again (3.23) in combination with (3.17) and (3.13), inserting $\pm a_2(c_h^{n+1}; c(t_{n+1}), \xi_c^{n+1})$ and $\pm a_2(\mathcal{I}_h c^{n+1}; c(t_{n+1}), \xi_c^{n+1})$; we have

$$\begin{aligned}
|\hat{I}_5| &\leq \frac{\hat{C}_a^2 \tau h^{2k}}{2\varepsilon_4} \|c\|^2_{L^\infty(0,T;H^{k+1}(\Omega))} + \frac{\tau\varepsilon_4}{2} \|\xi_c^{n+1}\|^2_{1,\Omega} + \hat{C}_{\text{lip}} M \|\xi_c\|^2_{1,\Omega} \\
&\quad + \frac{\tilde{C}_{\text{lip}}^2 M^2 \tau h^{2k}}{2\varepsilon_5} \|c\|^2_{L^\infty(0,T;H^k(\Omega))} + \frac{\varepsilon_5 \tau}{2} \|\xi_c^{n+1}\|^2_{1,\Omega}.
\end{aligned}$$

In order to derive a bound for $\hat{I}_6$ we add and subtract the terms

$$\pm c_2(\boldsymbol{u}(t_{n+1}), \mathcal{I}_h c(t_{n+1}), \xi_c^{n+1}), \quad \pm c_2(\Pi_h \boldsymbol{u}(t_{n+1}), \mathcal{I}_h c(t_{n+1}), \xi_c^{n+1}), \quad \pm c_2(\Pi_h \boldsymbol{u}(t_{n+1}), c(t_{n+1}), \xi_c^{n+1}),$$

which yields

$$\begin{aligned}
\hat{I}_6 = 4\tau \big(& c_2^h(\boldsymbol{u}_h^{n+1}, \mathcal{I}_h c(t_{n+1}), \xi_c^{n+1}) - c_2(\Pi_h \boldsymbol{u}(t_{n+1}), \mathcal{I}_h c(t_{n+1}), \xi_c^{n+1}) \\
&+ c_2(\Pi_h \boldsymbol{u}(t_{n+1}), \mathcal{I}_h c(t_{n+1}), \xi_c^{n+1}) - c_2(\Pi_h \boldsymbol{u}(t_{n+1}), c(t_{n+1}), \xi_c^{n+1}) \\
&+ c_2^h(\Pi_h \boldsymbol{u}(t_{n+1}), c(t_{n+1}), \xi_c^{n+1}) - c_2(\boldsymbol{u}(t_{n+1}) c(t_{n+1}), \xi_c^{n+1}) + c_2(\boldsymbol{u}_h^{n+1}, \xi_c^{n+1}, \xi_c^{n+1}) \big).
\end{aligned}$$

Using (3.19), (3.12c) and (3.23), we get

$$\begin{aligned}
|\tilde{I}_6| \leq 4\tau \bigg(& \frac{\tilde{C}^2 C^*}{2\varepsilon_6} \|\xi_{\boldsymbol{u}}^{n+1}\|^2_{1,\mathcal{T}_h} \|c\|^2_{L^\infty(0,T;H^1(\Omega))} + \frac{\varepsilon_6}{2} \|\xi_c\|^2_{1,\Omega} + \frac{h^{2k} C \tilde{C}^2}{2\varepsilon_7} \|\boldsymbol{u}\|^2_{L^\infty(0,T;\mathbf{H}^1(\Omega))} \|c\|^2_{L^\infty(0,T;H^{k+1}(\Omega))} \\
&+ \frac{\varepsilon_7}{2} \|\xi_c^{n+1}\|^2_{1,\Omega} + \frac{C h^{2k} \tilde{C}^2}{2\varepsilon_8} \|\boldsymbol{u}\|^2_{L^\infty(0,T;\mathbf{H}^{k+1}(\Omega))} \|c\|^2_{L^\infty(0,T;H^1(\Omega))} + \frac{\varepsilon_8}{2} \|\xi_c^{n+1}\|^2_{1,\Omega} \bigg).
\end{aligned}$$

Now, using (3.20) and (3.28), we have:

$$\begin{aligned}
|\hat{I}_7| &\leq \frac{C_d^2}{\varepsilon_9} 2\tau \big(C^* h^{2k} \|c\|^2_{L^\infty(0,T;H^k(\Omega))} + \|\xi_c\|^2_{0,\Omega} \big) + 2\tau\varepsilon_9 \|\xi_c^{n+1}\|^2_{1,\Omega}, \\
|\hat{I}_8| &\leq \frac{\gamma_3^2}{\varepsilon_{10}} 2\tau \big(C^* h^{2k} \|c\|^2_{L^\infty(0,T;H^k(\Omega))} + \|\xi_c\|^2_{0,\Omega} \big) + 2\tau\varepsilon_{10} \|\xi_c^{n+1}\|^2_{1,\Omega}.
\end{aligned}$$

In this manner, and after choosing $\varepsilon_i = 4\hat{\alpha}_a/25$ for $i = 1, \ldots, 8$ and $M \leq \hat{\alpha}_a/\hat{C}_{\text{Lip}}$, we can collect the above estimates and sum over $1 \leq n \leq m$, for all $m + 1 \leq N$, to get

$$\begin{aligned}
&\|\xi_c^{m+1}\|^2_{0,\Omega} + \|2\xi_c^{m+1} - \xi_c^m\|^2_{0,\Omega} + \sum_{n=1}^m \|\Lambda \xi_c^n\|^2_{0,\Omega} + \sum_{n=1}^m \tau\hat{\alpha}_a \|\xi_c^{n+1}\|^2_{1,\Omega} - 3\|\xi_c^1\|^2_{0,\Omega} \\
&\leq C(\tau^4 + h^{2k}) + \sum_{n=1}^m \eta_2 \|\xi_{\boldsymbol{u}}^{n+1}\|^2_{1,\mathcal{T}_h} + \sum_{n=1}^m \tau \frac{25}{\hat{\alpha}_a} (C_d^2 + \gamma_3^2) \|\xi_c\|^2_{0,\Omega}.
\end{aligned}$$

And the proof is completed by considering τ sufficiently small and applying Gronwall's lemma. $\quad\square$

Theorem 3.5. *Under the assumptions of Theorems 3.3 and 3.4 with*

$$M := \min\left\{ \frac{\tilde{\alpha}_a}{\hat{C}_{\text{Lip}}}, \frac{\tilde{\alpha}_a}{4\tilde{C}_u C^* C_\infty} \right\}$$

there exist positive constants $\hat{\gamma}_u$ and $\hat{\gamma}_c$ independent of τ and h, such that for a sufficiently small τ and all $m+1 \leq N$, the following inequalities hold

$$\left(\|\xi_{\boldsymbol{u}}^{m+1}\|^2_{0,\Omega} + \|2\xi_{\boldsymbol{u}}^{m+1} - \xi_{\boldsymbol{u}}^m\|^2_{0,\Omega} + \sum_{n=1}^m \|\Lambda \xi_{\boldsymbol{u}}^n\|^2_{0,\Omega} + \sum_{n=1}^m \tau\tilde{\alpha}_a \|\xi_{\boldsymbol{u}}^{n+1}\|^2_{1,\mathcal{T}_h} \right)^{1/2} \leq \hat{\gamma}_u(\tau^2 + h^k),$$

$$\left(\|\xi_c^{m+1}\|^2_{0,\Omega} + \|2\xi_c^{m+1} - \xi_c^m\|^2_{0,\Omega} + \sum_{n=1}^m \|\Lambda \xi_c^n\|^2_{0,\Omega} + \sum_{n=1}^m \tau\hat{\alpha}_a \|\xi_c^{n+1}\|^2_{1,\Omega} \right)^{1/2} \leq \hat{\gamma}_c(\tau^2 + h^k).$$

Proof. From Theorem 3.3 we have the estimate

$$\sum_{n=1}^{m} \tau \|\xi_{\boldsymbol{u}}^{n+1}\|_{1,\mathcal{T}_h}^2 \leq C(\tau^4 + h^{2k}) + \frac{\eta_1}{\tilde{\alpha}_a} \sum_{n=1}^{m} \tau \|\xi_c^{n+1}\|_{0,\Omega}^2,$$

which, substituting back into Theorem 3.4, yields

$$\|\xi_c^{m+1}\|_{0,\Omega}^2 + \|2\xi_c^{m+1} - \xi_c^m\|_{0,\Omega}^2 + \sum_{n=1}^{m} \|\Lambda\xi_c^n\|_{0,\Omega}^2 + \sum_{n=1}^{m} \tau\hat{\alpha}_a \|\xi_c^{n+1}\|_{1,\Omega}^2$$

$$\leq C(\tau^4 + h^{2k}) + \frac{\eta_1\eta_2}{\tilde{\alpha}_a} \sum_{n=1}^{m} \tau \|\xi_c^{n+1}\|_{0,\Omega}^2.$$

For the last term on the right-hand side of this last bound we have

$$\|\xi_c^{m+1}\|_{0,\Omega}^2 \leq 2\big(\|\Lambda\xi_c^m\|_{0,\Omega}^2 + \|2\xi_c^m - \xi_c^{m-1}\|_{0,\Omega}^2\big),$$

and considering τ sufficiently small and applying Gronwall's lemma, we readily deduce that

$$\|\xi_c^{m+1}\|_{0,\Omega}^2 + \|2\xi_c^{m+1} - \xi_c^m\|_{0,\Omega}^2 + \sum_{n=1}^{m} \|\Lambda\xi_c^{n+1}\|_{0,\Omega}^2 + \sum_{n=1}^{m} \tau\hat{\alpha}_a \|\xi_c^{n+1}\|_{1,\Omega}^2 \leq C(\tau^4 + h^{2k}). \tag{3.38}$$

The first bound follow by combining (3.38) and Theorem 3.3. $\quad\square$

Lemma 3.3. *Under the same assumptions of Theorem 3.5, we have*

$$\left(\sum_{n=1}^{m} \tau \|p(t_{n+1}) - p_h^{n+1}\|_{0,\Omega}^2\right)^{1/2} \leq \hat{\gamma}_p(\tau^2 + h^k).$$

Proof. Owing to the inf–sup condition (3.21), there exists a function $\boldsymbol{w}_h \in \mathbf{X}_h^\perp$ such that

$$b\big(\boldsymbol{w}_h, p(t_{n+1}) - p_h^{n+1}\big) = \|p(t_{n+1}) - p_h^{n+1}\|_{0,\Omega}^2, \tag{3.39}$$

$$\|\boldsymbol{w}_h\|_{1,\mathcal{T}_h} \leq \frac{1}{\tilde{\beta}} \|p(t_{n+1}) - p_h^{n+1}\|_{0,\Omega}. \tag{3.40}$$

From (3.9) and Lemma 3.2, proceeding as in the proof of Theorem 3.3, we obtain

$$\tau b(\boldsymbol{w}_h, p(t_{n+1}) - p_h^{n+1}) = -\tau \left(\boldsymbol{u}'(t_{n+1}) - \frac{3\boldsymbol{u}_h^{n+1} - 4\boldsymbol{u}_h^n + \boldsymbol{u}_h^{n-1}}{2\tau}, \boldsymbol{w}_h\right)_\Omega$$

$$+ \tau\big(a_1^h(c_h^{n+1}; \boldsymbol{u}_h^{n+1}, \boldsymbol{w}_h) - a_1^h(c(t_{n+1}); \boldsymbol{u}(t_{n+1}), \boldsymbol{w}_h)\big)$$

$$+ \tau\big(c_1^h(\boldsymbol{u}_h^{n+1}; \boldsymbol{u}_h^{n+1}, \boldsymbol{w}_h) - c_1^h(\boldsymbol{u}(t_{n+1}); \boldsymbol{u}(t_{n+1}), \boldsymbol{w}_h)\big)$$

$$+ \tau\big(\mathbf{F}_g(c(t_{n+1}), \boldsymbol{w}_h) - \mathbf{F}_g(c_h^{n+1}, \boldsymbol{w}_h)\big) + \tau\big(\mathbf{F}_r(\boldsymbol{u}(t_{n+1}), \boldsymbol{w}_h) - \mathbf{F}_r(\boldsymbol{u}_h^{n+1}, \boldsymbol{w}_h)\big)$$

$$\leq \frac{\tau^2}{2\sqrt{3}} \|\boldsymbol{u}^{(3)}\|_{L^2(t_{n-1}, t_{n+1}, \mathbf{L}^2(\Omega))} \sqrt{\tau} \|\boldsymbol{w}_h\|_{1,\mathcal{T}_h}$$

$$+ \tilde{C}_a C^* h^k \tau \|\boldsymbol{u}\|_{L^\infty(0,T;\mathbf{H}^{k+1}(\Omega))} \|\boldsymbol{w}_h\|_{1,\mathcal{T}_h} + \tilde{C}_{\text{lip}} M \tau \|\xi_c^{n+1}\|_{1,\Omega} \|\boldsymbol{w}_h\|_{1,\mathcal{T}_h}$$

$$+ \tilde{C}_{\text{lip}} \tau M \|\xi_c\|_{1,\Omega} \|\boldsymbol{w}_h\|_{1,\mathcal{T}_h} + \tau C \tilde{C}_u C^* C_\infty M \|\xi_c\|_{1,\Omega} \|\boldsymbol{w}_h\|_{1,\mathcal{T}_h}$$

$$+ \tau C \tilde{C}_u h^k \|\boldsymbol{u}\|_{L^\infty(0,T;\mathbf{H}^1(\Omega))} \|\boldsymbol{u}\|_{L^\infty(0,T;\mathbf{H}^{k+1}(\Omega))} \|\boldsymbol{w}_h\|_{1,\mathcal{T}_h}$$

$$+ \tau C \tilde{C}_u h^k \|\boldsymbol{u}\|_{L^\infty(0,T;\mathbf{H}^1(\Omega))} \|\boldsymbol{u}\|_{L^\infty(0,T;\mathbf{H}^{k+1}(\Omega))} \|\boldsymbol{w}_h\|_{1,\mathcal{T}_h}$$

$$+ \gamma_2 \tau h^k C^* \|c\|_{L^\infty(0,T;H^k(\Omega))} \|\boldsymbol{w}_h\|_{1,\mathcal{T}_h} + \gamma_2 \tau \|\xi_{\boldsymbol{u}}\|_{0,\Omega} \|\boldsymbol{w}_h\|_{1,\mathcal{T}_h}$$

$$+ \gamma_1 \tau h^k C^* \|\boldsymbol{u}\|_{L^\infty(0,T;\mathbf{H}^k(\Omega))} \|\boldsymbol{w}_h\|_{1,\mathcal{T}_h} + \gamma_1 \tau \|\xi_{\boldsymbol{u}}\|_{0,\Omega} \|\boldsymbol{w}_h\|_{1,\mathcal{T}_h}.$$

Table 4.1
Spatial accuracy test: experimental errors and convergence rates for the approximate solutions $\boldsymbol{u}_h$, p_h and c_h. Values are displayed for schemes with first and second order in space.

k	DoF	$e_{\boldsymbol{u}}$	rate	e_p	rate	e_s	rate
1	53	0.004507	–	0.291804	–	0.253207	–
	299	0.002783	0.679	0.192100	0.589	0.153518	0.708
	1 265	0.001273	1.150	0.096891	1.006	0.073370	1.085
	4 634	0.000631	1.017	0.051713	0.911	0.038362	0.941
	17 780	0.000308	1.033	0.026853	0.945	0.018841	1.026
2	132	0.001817	–	0.115142	–	0.089672	–
	797	0.000342	2.349	0.032084	1.799	0.018151	2.249
	3 427	8.031e−5	2.133	0.007198	2.197	0.003702	2.337
	12 702	1.948e−5	2.056	0.002023	1.844	0.000996	1.905
	49 157	4.358e−6	2.159	0.000525	1.941	0.000251	1.987

Summing over $1 \le n \le m$ for all $m + 1 \le N$ and substituting back into Eqs. (3.39) and (3.40), we obtain

$$\left(\sum_{n=1}^{m} \tau \| p(t_{n+1}) - p_h^{n+1} \|_{0,\Omega}^2 \right)^{1/2} \le \frac{C}{\tilde{\beta}} \left((\tau^2 + h^k) + \left(\sum_{n=1}^{m} \tau \| \xi_c^{n+1} \|_{0,\Omega}^2 \right)^{1/2} + \left(\sum_{n=1}^{m} \tau \| \xi_{\boldsymbol{u}}^{n+1} \|_{1,\mathcal{T}_h}^2 \right)^{1/2} \right).$$

The result follows by applying Theorem 3.5. □

4. Numerical results

In this section we test the performance of the numerical method and produce some typical solutions in operating conditions. Tetrahedral meshes have been constructed using the freely available mesh manipulator GMSH [35], and the implementation of the H(div)-conforming finite element scheme is carried out using the open source finite element library FEniCS [36]. The linear systems encountered at each Newton–Raphson step are solved with the GMRES method preconditioned with AMG. The Newton iterations stop whenever either the absolute or the relative residuals (measured in the ℓ^2−norm) drop below the fixed tolerance set to 1×10^{-6}. Apart from the main python modules, a dedicated C++ expression is needed to efficiently compile the position of the rake at each time. It depends on the structure dimensions and on the angular velocity.

4.1. Numerical verification of convergence

We start with a simple experimental convergence analysis to confirm the error bounds anticipated in Section 3.2. Doing this in a 2D domain suffices, so we consider Ω as a circle of radius one and construct a sequence of successively refined meshes on which we compute errors between the approximate solutions obtained with the H(div)-conforming scheme and the closed-form solutions

$$\boldsymbol{u} = \sin(t) \begin{pmatrix} \cos(\pi/2x)\sin(\pi/2y) \\ -\sin(\pi/2x)\cos(\pi/2y) \end{pmatrix}, \quad p = (x^4 - y^4)\exp(-t), \quad c = \frac{1}{2}\cos\left(\frac{\pi}{4}|\boldsymbol{x}|^2\right)\exp(-t),$$

that are used to construct suitable Dirichlet boundary data for velocity and an exact flux for concentration, and manufactured forcing and source terms $\mathbf{F}_{ex}$ and g_{ex} appearing on the right-hand side of the momentum equation and of the concentration mass balance, respectively. As $\boldsymbol{u}$ is prescribed everywhere on $\partial\Omega$, for sake of uniqueness we impose $p \in L_0^2(\Omega)$ through a Lagrange multiplier approach. We use a constant viscosity $\nu = 0.01$ and diffusivity $D = 1.0$ with $\boldsymbol{f}_r$ as given in (3.25), $f_{bk}(c) = 1 \times 10^{-2}(1 - c)$ and $\boldsymbol{k}$ pointing in the radial outwards direction.

We show orders of convergence in the discrete norm $\| \cdot \|_{1,\mathcal{T}_h}$ for the velocity $\boldsymbol{u}$, in the L^2-norm of the error of p, and in the H^1-norm of the error in c in Table 4.1. For polynomial degrees $k = 1$ and $k = 2$ we observe that the order of convergence predicted by our theory (see Theorem 3.5 and Lemma 3.3) is achieved.

Table 4.2
Time accuracy test: experimental errors and convergence rates for the approximate solutions u_h, p_h and c_h, computed for each refinement level.

τ	$\hat{e}_u$	rate	$\hat{e}_p$	rate	$\hat{e}_s$	rate
2	5.6194	–	0.5069	–	0.4558	–
1	1.5943	1.817	0.1809	1.487	0.0868	2.391
0.5	0.4433	1.847	0.0523	1.789	0.0193	2.167
0.25	0.1153	1.943	0.0135	1.951	0.0046	2.070
0.125	0.0296	1.959	0.0033	2.000	0.0012	1.994
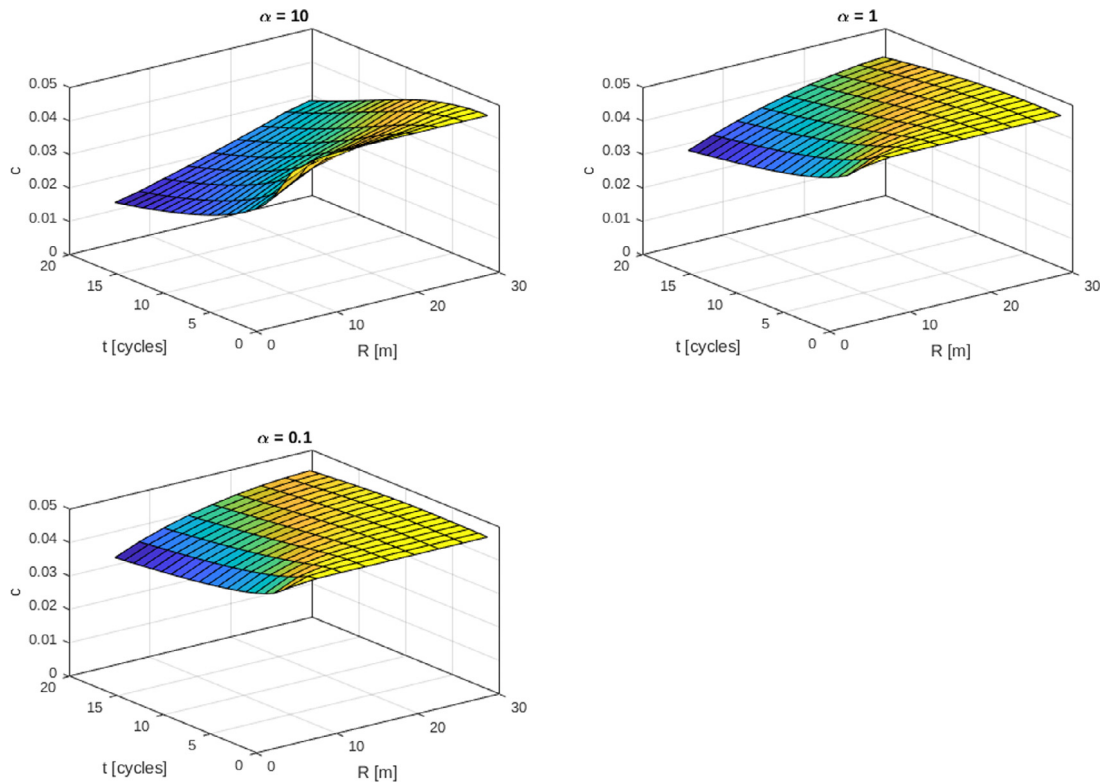
Fig. 4.1. Spatio-temporal variation of the average concentration after complete rake cycles at different radius (measured from the centre of the annular domain) and values of α.

Regarding the convergence of the time advancing scheme, now we set $T = 4$ and consider a sequence of uniform refined time partitions τ_l, $l \in \{1, 2, 3, 4, 5\}$ where the time step is 2^{2-l}. Absolute errors are computed as

$$\hat{e}_u = \left(\sum_{n=1}^{m} \tau \| u(t_{n+1}) - u_h^{n+1} \|_{1,\mathcal{T}_h}^2 \right)^{1/2}, \quad \hat{e}_p = \left(\sum_{n=1}^{m} \tau \| p(t_{n+1}) - p_h^{n+1} \|_{0,\Omega}^2 \right)^{1/2},$$

$$\hat{e}_c = \left(\sum_{n=1}^{m} \tau \| c(t_{n+1}) - c_h^{n+1} \|_{1,\Omega}^2 \right)^{1/2},$$

and we readily observe from Table 4.2 that the method converges to the exact solution with the expected second-order rate.
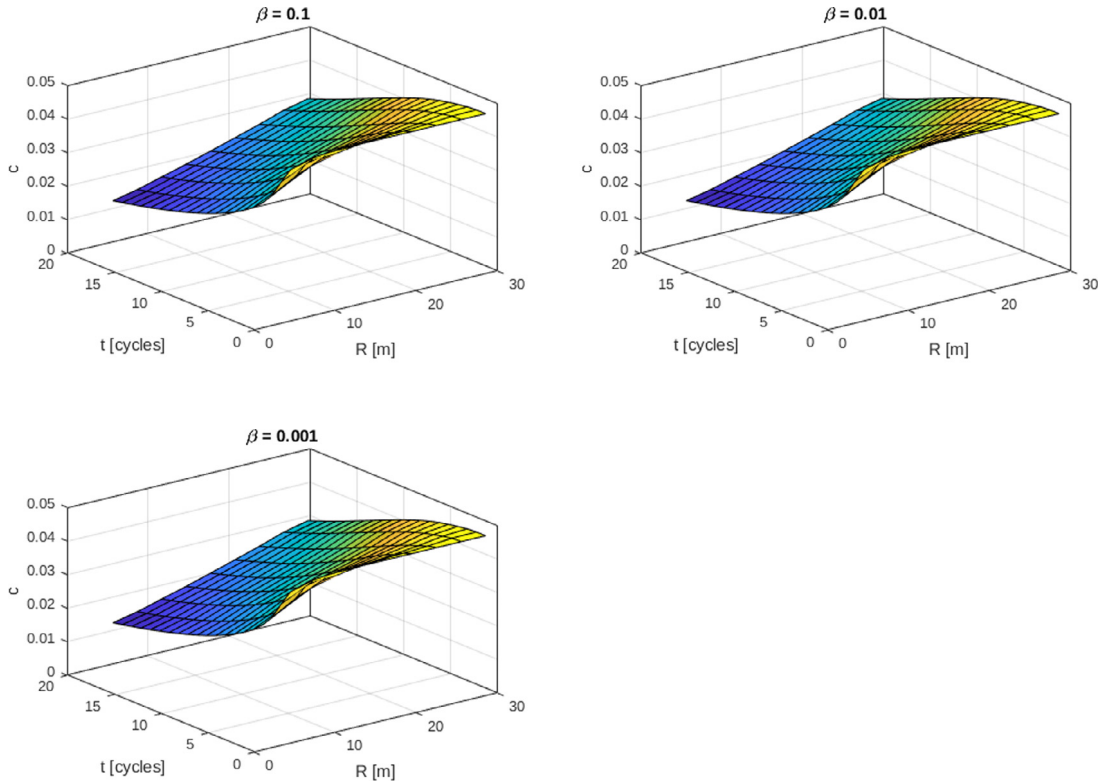
Fig. 4.2. Spatio-temporal variation of the average concentration after complete rake cycles at different radius (measured from the centre of the annular domain) and values of β.

4.2. Preliminary two-dimensional computation

The typical operation conditions in the clarifier–thickener unit are characterised by about 1.2 revolutions per hour, a solid concentration behind the rake of 0.01 g/l, a feed flow rate of 10,000 gpm, a return sludge flow rate of 3000 gpm, an effluent flow rate in the overflow weir of approximately 7000 gpm, and a solid concentration at the inlet of 5 g/l (see [3] and the references therein). The specification of the remaining model parameters, at least in this specific scenario, are much less clear and we need to characterise them in terms of the expected flow conditions. Known issues in the operation process include a strong backflow into the feedwell, a large recirculation zone near the feedwell, the high velocity of the flow exiting the feedwell, and the lack of flow symmetry.

In order to gain insight into the impact of the rake parameters on the simulation we regard the operation from an azimuthal view and consider only the coupled Navier–Stokes/concentration problem in an annular domain of external radius 30 m and internal radius 3 m, where one can still see the rotating arm, but the vertical sedimentation is not represented. Here the body force term exerted on the fluid ($\mathbf{F}_g$) is considered with a radial direction towards the centre of the inner disk. Furthermore the parameters of the simulation are taken as follows:

$$\rho_s = 2500 \,\text{kg/m}^3, \quad c_0 = 0.05, \quad \rho_f = 1000 \,\text{kg/m}^3, \quad \omega = 1.2 \,\text{rad/min}, \quad c_r = 1 \times 10^{-3},$$
$$g = 1 \times 10^{-3} \,\text{m/min}^2, \quad D_0 = 1.0 \,\text{m}^2/\text{min}, \quad \nu_0 = 0.05 \,\text{kg/(m min)},$$
$$f_{bk}(c) = 1.0 \times 10^{-3} c(1-c)^2 \,\text{m/s}, \quad \sigma_e(c) = \begin{cases} 0 & \text{for } c \leq c_c = 0.07, \\ (50.0/c_c)((c/0.07)^5 - 1) \,\text{Pa} & \text{for } c > c_c. \end{cases}$$

We start the simulation with a homogeneous initial concentration c_0 and then, we observe how this concentration changes over time for different values of the parameters α and β. From results shown in Figs. 4.1 and 4.2 it can be highlighted that the solids removal coefficient α is the most relevant for the concentration profile, while the combined contributions from drag and density do not seem to have an appreciable effect. Precisely, Fig. 4.1 indicates that solids
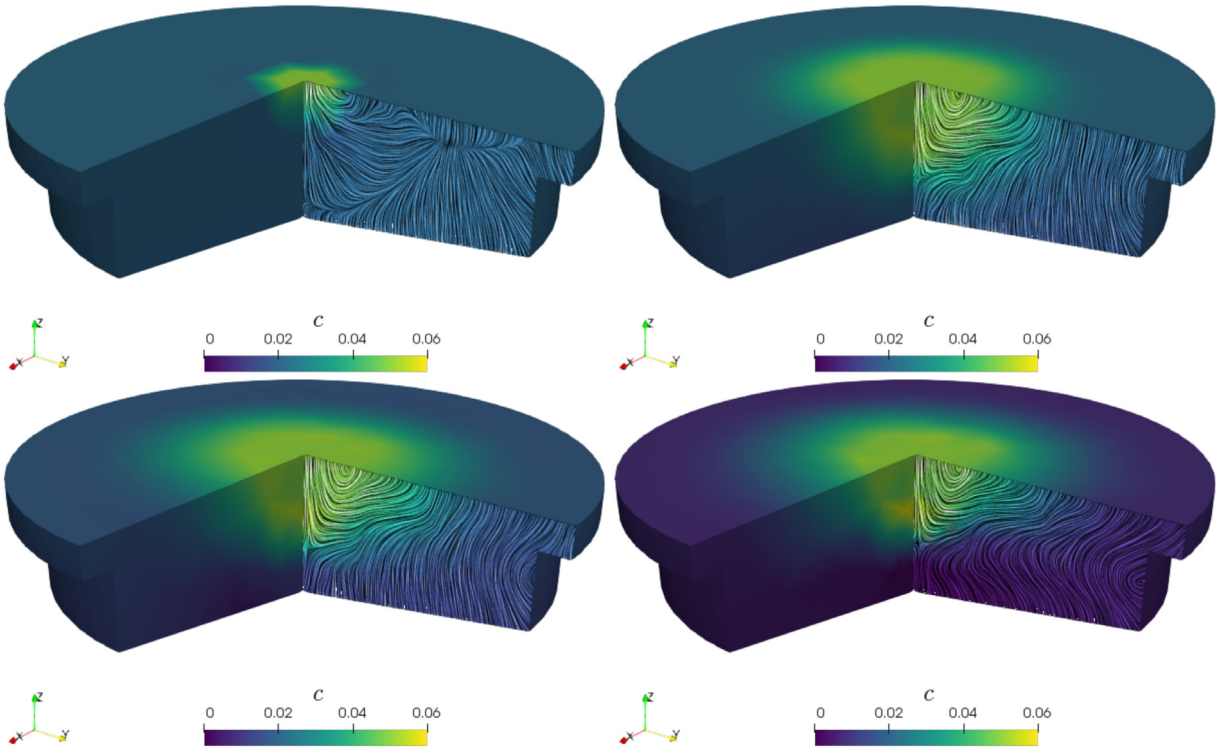
Fig. 4.3. Domain cuts showing snapshots of solids concentration and line integral contours of velocity on a slice, focusing on time instants $t = 1, 30, 60$ and 180 [min].

concentrations near the outlet, that is, the centre of rotation, diminish more rapidly in time for large values of α, as can be inferred, for example, comparing the result for $\alpha = 10$ with that for $\alpha = 0.1$. These results confirm that within the simulation model the parameter α controls the total solid mass removed. This parameter should therefore carefully be tuned when the model is applied to a real system. On the other hand that the results are nearly the same for three values of β considered (see Fig. 4.2) explains that this term, which quantifies the momentum loss due to drag, does not influence the attainable solids concentrations, but may become important for the determination of the torque necessary to move the rake (this quantity is not included in our analysis here).

4.3. Performance of clarifier units

Having now a better understanding on the dimension and isolated effects of each mechanism in the coupled problem, we turn to the simulation of the sedimentation of flocculated suspensions in a more realistic geometry. We consider the domain sketched in Fig. 1.1, and take $R = 15$ m and $H = 7$ m. We suppose that the tank is initially filled with a homogeneous mixture of concentration $c_0 = 0.02$. Apart from the specifications in (2.2), (2.3), the remaining concentration-dependent and constant parameters needed in the model assume the following form (where the suspension is assumed of type *Kaolin flat D*)

$$\rho_s = 2500\,\text{kg/m}^3, \quad c_{in} = 0.05, \quad \rho_f = 1000\,\text{kg/m}^3, \quad \omega = 0.12\,\text{rad/min}, \quad \alpha = 0.01\,\text{min}^{-1},$$

$$\beta\rho_r = 50\,\text{kg/m}^3\,\text{m}^{-1}, \quad c_r = 1 \times 10^{-3}, \quad g = 9.8\,\text{m/s}^2, \quad D_0 = 0.05\,\text{m}^2/\text{min},$$

$$\boldsymbol{u}_{in} = -4.2\boldsymbol{k}\,\text{m/min}, \quad \nu_0 = 0.05\,\text{kg/(m min)},$$

$$f_{bk}(c) = 1.0 \times 10^{-4}c(1-c)^2\,\text{m/s}, \quad \sigma_e(c) = \begin{cases} 0 & \text{for } c \leq c_c = 0.07, \\ (50.0/c_c)((c/0.07)^5 - 1)\,\text{Pa} & \text{for } c > c_c. \end{cases}$$

We conduct a series of runs on the 3D geometry where the resulting tetrahedral mesh has 139 001 elements and 27 510 vertices (representing 1.1M DoFs for the lowest-order H(div)-conforming finite element method). The time
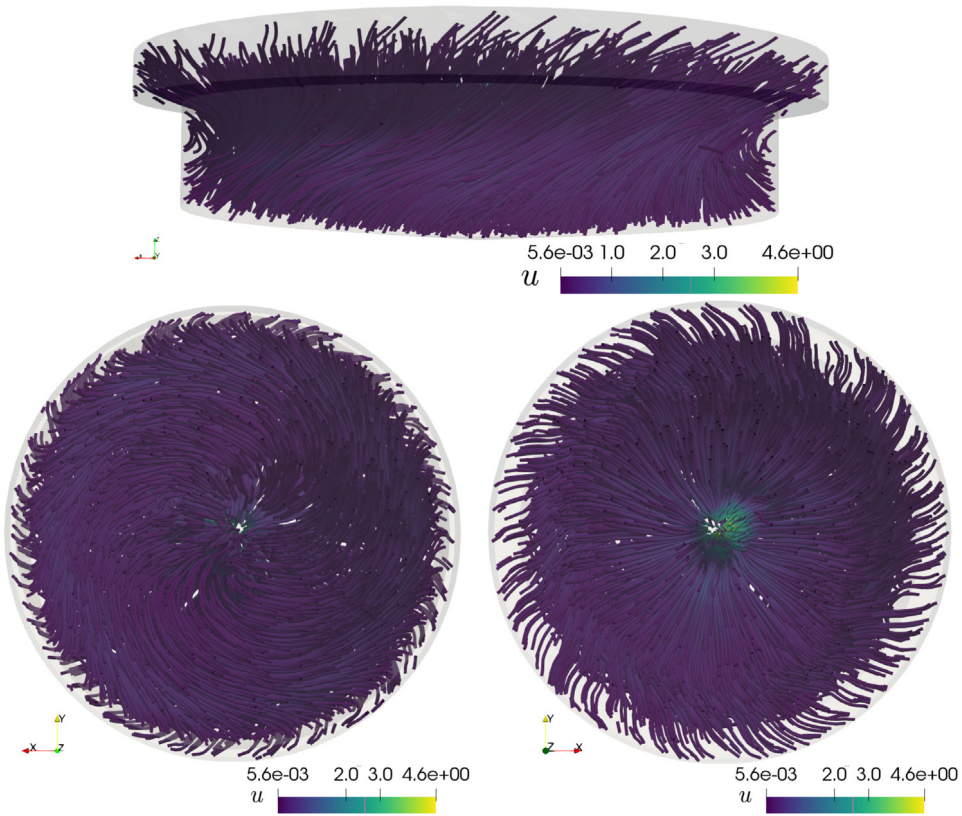
Fig. 4.4. Velocity streamlines at 180 [min], shown from the side (top panel), from the bottom (bottom left figure), and from the top (bottom right figure).

stepping scheme uses a fixed timestep of $\tau = 0.5$ min and we simulate the process until 180 min. As mentioned above, one manifestation of performance in the clarifier units is the development of recirculation patterns, and we plot in Fig. 4.3 the concentration profiles on a cut of the domain, as well as a slice of a section where we plot line integral contours of velocity, for three different times. The plots indicate a large diffusion of the concentration as it spreads out from the feedwell, and we also see a substantial modification on the flow patterns due to the combined contribution of the rake mechanism and the gravitational settling. The velocity can be seen more clearly from Fig. 4.4, showing streamlines at $t = 180$ min from different angles, emphasising that the recirculation in the (x, y)-plane occurs mainly near the bottom of the vessel, whereas on the top the velocity is dominated by gravitational forces and a radially spreading concentration-driven flow.

On the other hand, the variation of the flow conditions depending on different factors can be observed from Figs. 4.5, 4.6, and 4.7. There we portray the dynamics of the concentration and flow rate on the overflow, that is, respectively

$$\frac{1}{60\pi} \int_{\Gamma_{\mathrm{ofl}}} c \, \mathrm{d}s, \qquad \frac{1}{60\pi} \int_{\Gamma_{\mathrm{ofl}}} \boldsymbol{u} \cdot \boldsymbol{n} \, \mathrm{d}s,$$

according to modifications in the solids removal intensity, on the drag and density of the rotating rake, and on the rake height. Based on the results of this set of simulations, we can identify the solids removal coefficient α as the most sensitive factor on the outputs of overflow concentration and overflow flow rate. On the other hand, the combined contributions from drag and density do not seem to have a large effect on these markers, which is consistent with what we saw in the preliminary 2D test. However, a further inspection reveals that the effects are not necessarily localised but they differ over the height of the device. From Fig. 4.8 we can see how the average concentration varies over time (and measured after a given number of cycles of the rotating rake) depending on the solids removal coefficient and on the drag.
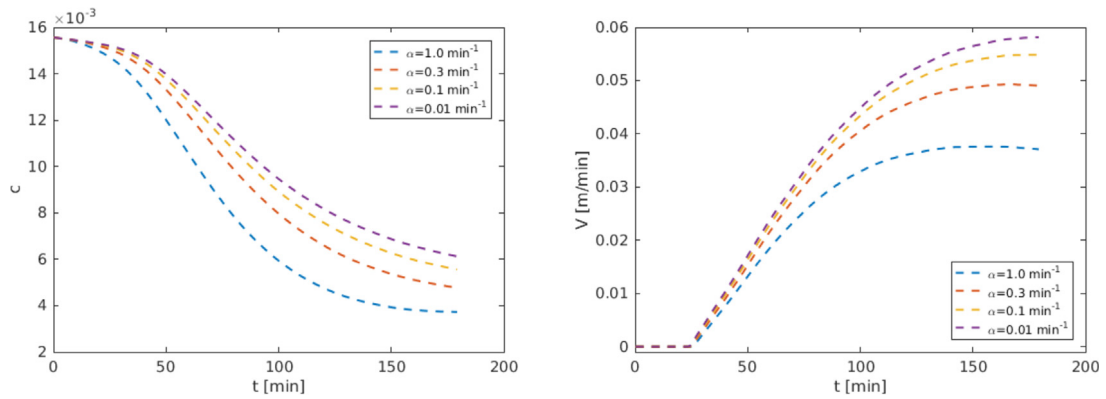
Fig. 4.5. Time evolution of the concentration and normal velocity on the overflow for different values of the solids removal coefficient α.
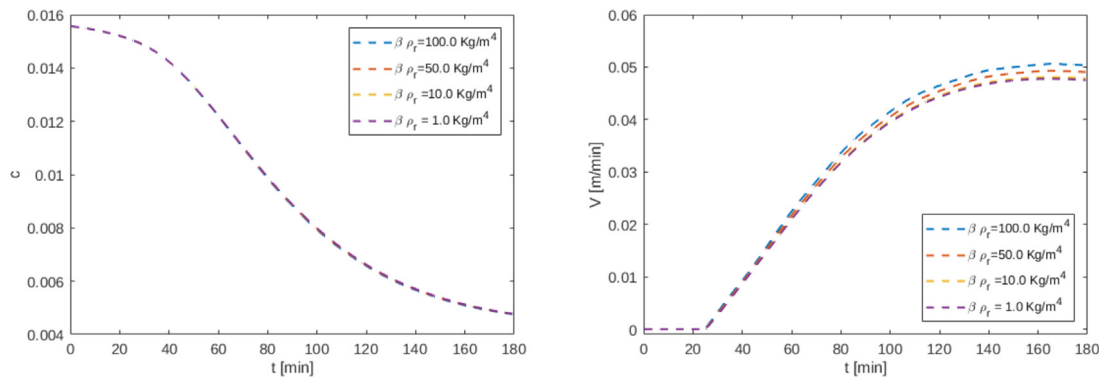

Fig. 4.6. Time evolution of the concentration and normal velocity on the overflow for different values of the drag-density coefficient $\beta\rho_r$.
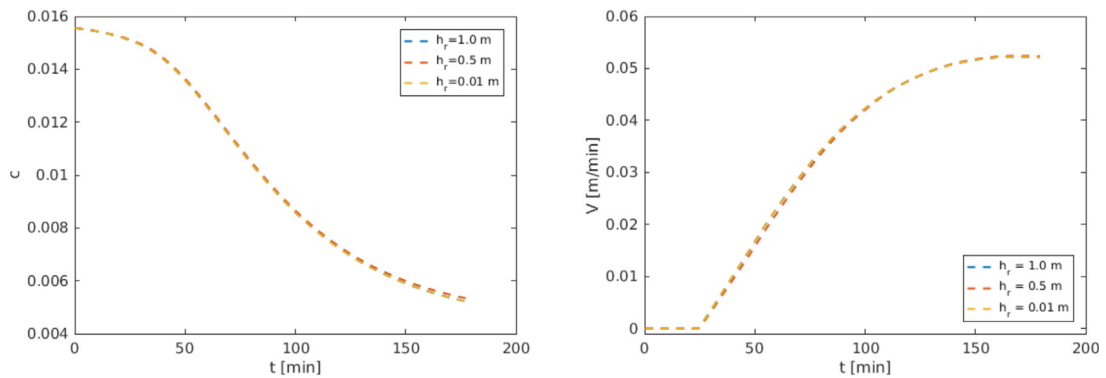

Fig. 4.7. Time evolution of the concentration and normal velocity on the overflow for different values of rake height h_r.

5. Discussion and concluding remarks

We have advanced a model for the process of clarification and thickener in circular units in the presence of a spinning rake structure. The model is intrinsically 3D, it incorporates a detailed flow-sedimentation coupling in the settling mixture and it considers a simplified, one-way coupling that only imposes the velocity of the rotating arm which affects both the transport of solid particles and the revolving flow near the bottom of the tank. This addition constitutes an important generalisation over existing models for sedimentation–consolidation processes reviewed in
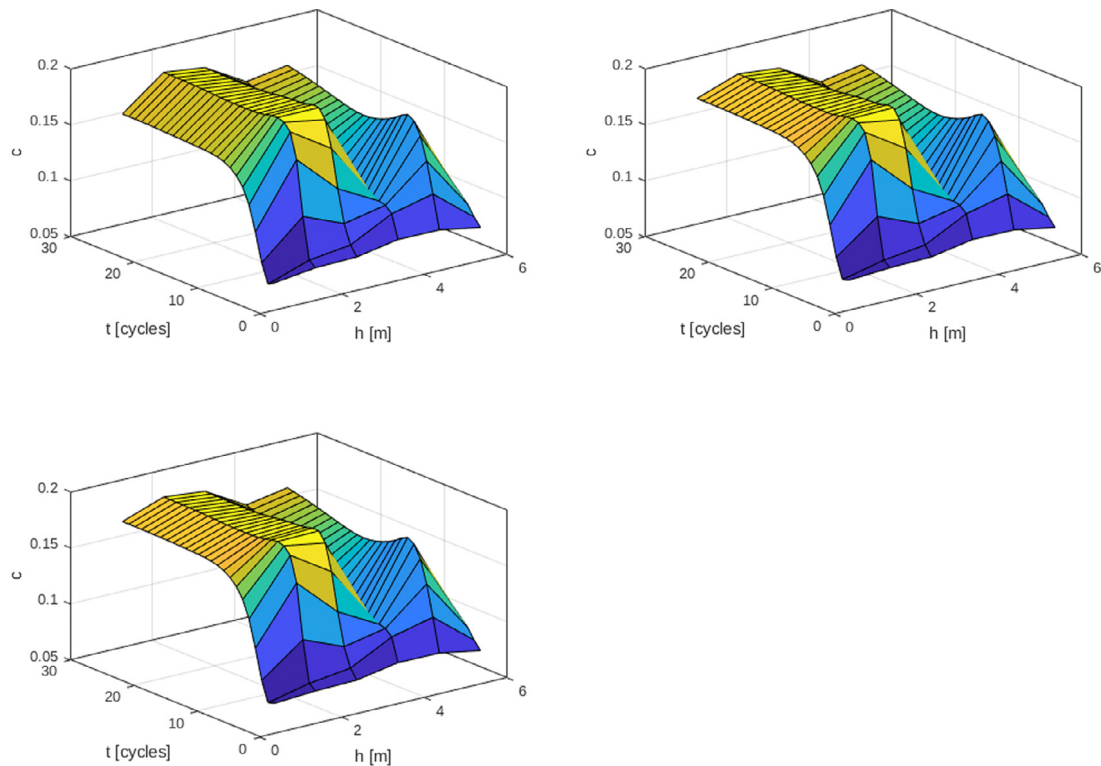
Fig. 4.8. Spatio-temporal variation of the average concentration after complete rake cycles at different heights (measured from the bottom) with $\alpha = 0.3$, $\beta = 50$ (top left), $\alpha = 0.0$, $\beta = 50$ (top right), $\alpha = 0.0$, $\beta = 0.0$ (bottom).

e.g. [37]. The numerical method we have used is based on H(div)-conforming finite element methods for the flow and classical Lagrange elements for the solids concentration. A monolithic Newton scheme with exact Jacobian has been employed in all cases, and we have generated several tests to confirm the accuracy of the method and have analysed several cases relevant to the process of clarification. We hope that this study helps in gaining a fuller understanding of the operating conditions in clarifier units.

Several interesting extensions are left to be explored. Regarding modelling aspects, we mention that the present approach is likely to be more suitable for the application to clarifiers in wastewater treatment, since for that application the rake can be moved more easily through compacted sludge. In contrast, the sediments formed by the settling of mineral suspension exhibit major resistance to the motion of the rake, and the torque that needs to be applied (that is, the cost of energy) [12] and the precise conditions under which the rake could brake are of utmost importance (a rake being stuck or broken represents a major shutdown of the industrial process) [14]. Our model currently does not resolve the stresses generated in the structure, which is a natural next step. While the approach (2.6) is a rough approximation of the experimental and numerical observation that "rake blades typically suck material behind them as they move as well as pushing material in front of them" [13, p. 102] one could also easily extend the present development to the case of more adequate rheological models for the suspension [1], partly including the effect of shear [8,9] and changes in floc structure [7,10,11]. In addition, for the flow regimes we have studied here, turbulent effects have little relevance but in some industrial settings this is crucial to resolve the separation of clear fluid and solid particles [3,38]. Model reduction and the consistent connection with solid-flux theory should also be considered eventually [39]. It is also left to consider strong degeneracy of diffusion in the concentration equation (allowing $D_0 = 0$) due to compression effects. The analysis in this case is much more involved, and some partial results from, e.g., [40–44] could be used as starting point.

On the other hand, there are a number of improvements we can add in terms of our numerical method. For instance, to concentrate in the design of partitioned solvers and efficient preconditioners needed for costly 3D computations with long time horizons [21]. We could also incorporate mixed formulations and space adaptivity

through residual-based a posteriori error indicators [45], and employ more advanced flux reconstruction techniques useful in the regimes of convection-dominated flows.

Declaration of competing interest

The authors declare that they have no known competing financial interests or personal relationships that could have appeared to influence the work reported in this paper.

Acknowledgement

References

[1] R. Bürger, W.L. Wendland, F. Concha, Model equations for gravitational sedimentation-consolidation processes, ZAMM Z. Angew. Math. Mech. 80 (2000) 79–92.

[2] R. Ruiz-Baier, I. Lunati, Mixed finite element – discontinuous finite volume element discretization of a general class of multicontinuum models, J. Comput. Phys. 322 (2016) 666–688.

[3] S. Das, H. Bai, C. Wu, J.H. Kao, B. Barney, M. Kidd, M. Kuettel, Improving the performance of industrial clarifiers using three-dimensional computational fluid dynamics, Eng. Appl. Comput. Fluid Mech. 10 (2016) 130–144.

[4] R. Bürger, P.E. Méndez, R. Ruiz-Baier, On H(div)-conforming methods for double-diffusion equations in porous media, SIAM J. Numer. Anal. 57 (2019) 1318–1343.

[5] D. Boffi, L. Gastaldi, A finite element approach for the immersed boundary method, Comput. Struct. 81 (2003) 491–501.

[6] L. Szalai, P. Krebs, W. Rodi, Simulation of flow in circular clarifiers with and without swirl, J. Hydraul. Eng. 120 (1994) 4–21.

[7] G.M. Channell, C.F. Zukoski, Shear and compressive rheology of aggregated alumna suspensions, AIChE J. 43 (1997) 1700–1708.

[8] B.R. Gladman, M. Rudman, P.J. Scales, The effect of shear on gravity thickening: Pilot scale modelling, Chem. Eng. Sci. 65 (2010) 4293–4301.

[9] K. Gustavsson, J. Oppelstrup, Consolidation of concentrated suspensions—numerical simulations using a two-phase model, Comput. Vis. Sci. 3 (2000) 39–45.

[10] K. Gustavsson, J. Oppelstrup, J. Eiken, Consolidation of concentrated suspensions—shear and irreversible floc structure rearrangement, Comput. Vis. Sci. 4 (2001) 61–66.

[11] D.R. Lester, M. Rudman, P.J. Scales, Macroscopic dynamics of flocculated colloidal suspensions, Chem. Eng. Sci. 65 (2010) 6362–6378.

[12] M. Rudman, K. Simic, D.A. Paterson, P. Strode, A. Brent, I.D. Šutalo, Raking in gravity thickeners, Int. J. Miner. Process. 86 (2008) 114–130.

[13] I.D. Šutalo, D.A. Paterson, M. Rudman, Flow visualization and computational prediction in thickener rake models, Miner. Eng. 16 (2003) 93–102.

[14] S. Teerikoski, Optimal control of clarifier-thickeners, Master Thesis in Engineering Physics, Mathematics and Computer Science, Uppsala University, Sweden, 2017.

[15] C. Wong, P.H. Trinh, S.J. Chapman, Shear-induced instabilities of flows through submerged vegetation, J. Fluid Mech. 891 (2020) A17.

[16] P. Angot, C.H. Bruneau, P. Fabrie, A penalization method to take into account obstacles in incompressible viscous flows, Numer. Math. 81 (1999) 497–520.

[17] D. Kolomenskiy, K. Schneider, A fourier spectral method for the Navier–Stokes equations with volume penalization for moving solid obstacles, J. Comput. Phys. 228 (2009) 5687–5709.

[18] D. Boffi, L. Gastaldi, Discrete models for fluid–structure interactions: the finite element immersed boundary method, Discrete Contin. Dyn. Syst. S 9 (2016) 89–107.

[19] M. Discacciati, D. Hacker, A. Quarteroni, S. Quinodoz, S. Tissot, F.M. Wurm, Numerical simulation of orbitally shaken viscous fluids with free surface, Internat. J. Numer. Methods Fluids 71 (2013) 294–315.

[20] K. Nikitin, M. Olshanskii, K. Terekhov, Y. Vassilevski, R. Yanbarisov, An adaptive numerical method for free surface flows passing rigidly mounted obstacles, Comput. Fluids 148 (2017) 56–68.

[21] S. Badia, F. Verdugo, Robust and scalable domain decomposition solvers for unfitted finite element methods, J. Comput. Appl. Math. 344 (2018) 740–759.

[22] K. Yang, P. Sun, L. Wang, J. Xu, L. Zhang, Modeling and simulations for fluid and rotating structure interactions, Comput. Methods Appl. Mech. Engrg. 311 (2016) 788–814.

[23] G.J. Kynch, A theory of sedimentation, Trans. Faraday Soc. 48 (1952) 166–176.

[24] R. Bürger, S. Kumar, R. Ruiz-Baier, Discontinuous finite volume element discretization for coupled flow–transport problems arising in models of sedimentation, J. Comput. Phys. 299 (2015) 446–471.

[25] G. Galdi, A.L. Silvestre, On the motion of a rigid body in a Navier–Stokes liquid under the action of a time-periodic force, Indiana Univ. Math. J. 58 (2009) 2805–2842.

[26] F. Brezzi, J. Douglas, L.D. Marini, Two families of mixed finite elements for second order elliptic problems, Numer. Math. 47 (1985) 217–235.

[27] J. Könnö, R. Stenberg, H(div)-conforming finite elements for the brinkman problem, Math. Models Methods Appl. Sci. 21 (2011) 2227–2248.

[28] D.N. Arnold, F. Brezzi, B. Cockburn, L.D. Marini, Unified analysis of discontinuous Galerkin methods for elliptic problems, SIAM J. Numer. Anal. 39 (2002) 1749–1779.

[29] V. Girault, B. Rivière, M.F. Wheeler, A discontinuous Galerkin method with nonoverlapping domain decomposition for the Stokes and Navier–Stokes problems, Math. Comp. 74 (2005) 53–84.

[30] O.A. Karakashian, W.N. Jureidini, A nonconforming finite element method for the stationary Navier–Stokes equations, SIAM J. Numer. Anal. 35 (1998) 93–120.

[31] D.A. Di Pietro, A. Ern, Mathematical Aspects of Discontinuous Galerkin Methods, in: Series Mathématiques et Applications, Springer-Verlag, Berlin, 2011.

[32] R. Oyarzúa, T. Qin, D. Schötzau, An exactly divergence-free finite element method for a generalized Boussinesq problem, IMA J. Numer. Anal. 34 (2014) 1104–1135.

[33] F. Brezzi, M. Fortin, Mixed and Hybrid Finite Element Methods, Springer Verlag, 1991.

[34] R. Aldbaissy, F. Hecht, G. Mansour, T. Sayah, A full discretisation of the time-dependent Boussinesq (buoyancy) model with nonlinear viscosity, Calcolo 55 (2018) 44, 1–29.

[35] C. Geuzaine, J.-F. Remacle, Gmsh: a three-dimensional finite element mesh generator with built-in pre- and post-processing facilities, Internat. J. Numer. Methods Engrg. 79 (2009) 1309–1331.

[36] M.S. Alnæs, J. Blechta, J. Hake, A. Johansson, B. Kehlet, A. Logg, C. Richardson, J. Ring, M.E. Rognes, G.N. Wells, The FEniCS project version 1.5, Arch. Numer. Softw. 3 (100) (2015) 9–23.

[37] R. Bürger, J. Careaga, S. Diehl, C. Mejías, R. Ruiz-Baier, Convection–diffusion-reaction and transport-flow problems motivated by models of sedimentation: some recent advances, in: B. Sirakov, P. de Souza, M. Viana (Eds.), Proceedings of the International Congress of Mathematicians, in: Invited Lectures, vol. IV, World Scientific, Singapore, 2018, pp. 3489–3514.

[38] D. Kleine, B.D. Reddy, Finite element analysis of flows in secondary settling tanks, Internat. J. Numer. Methods Engrg. 64 (2005) 849–876.

[39] S. Diehl, The solids-flux theory — confirmation and extension by using partial differential equations, Water Res. 42 (2008) 4976–4988.

[40] S. Berres, R. Bürger, K.H. Karlsen, E.M. Tory, Strongly degenerate parabolic-hyperbolic systems modeling polydisperse sedimentation with compression, SIAM J. Appl. Math. 64 (2003) 41–80.

[41] F. Betancourt, R. Bürger, K.H. Karlsen, A strongly degenerate parabolic aggregation equation, Commun. Math. Sci. 9 (2011) 711–742.

[42] R. Bürger, K.-K. Fjelde, K. Höfler, K.H. Karlsen, Central difference solutions of the kinematic model of settling of polydisperse suspensions and three-dimensional particle-scale simulations, J. Eng. Math. 41 (2001) 167–187.

[43] M. Ghilani, E.H. Quenjel, M. Saad, Positive control volume finite element scheme for a degenerate compressible two phase flow in anisotropic porous media, Comput. Geosci. 23 (2019) 55–79.

[44] M. Ibrahim, M. Saad, Weighted weak formulation for a nonlinear degenerate equation arising in chemotaxis or porous media, J. Math. Anal. Appl. 446 (2017) 945–969.

[45] M. Alvarez, G.N. Gatica, R. Ruiz-Baier, A posteriori error estimation for an augmented mixed-primal method applied to sedimentation-consolidation systems, J. Comput. Phys. 367 (2018) 332–346.